

"Dynamics Calculations Based on *Ab Initio* Potential Energy Surfaces," D. G. Truhlar, F. B. Brown, D. W. Schwenke, R. Steckler, and B. C. Garrett, in *Comparison of Ab Initio Quantum Chemistry with Experiment for Small Molecules*, edited by R. J. Bartlett (Reidel, Dordrecht, Holland, 1985), pp. 95-139.

DYNAMICS CALCULATIONS BASED ON AB INITIO POTENTIAL ENERGY SURFACES

Donald G. Truhlar, Franklin B. Brown, David W. Schwenke
and Rozeanne Steckler, Department of Chemistry,
University of Minnesota, Minneapolis, Minnesota 55455

Bruce C. Garrett, Chemical Dynamics Corporation,
Columbus, Ohio 43220

1. INTRODUCTION

One of the most exciting developments in theoretical chemistry in the last few years has been the production of ab initio potential energy surfaces by electronic structure calculations and the use of these surfaces for dynamics calculations. With accurate enough surfaces, these dynamics calculations may yield results that rival the accuracy attainable experimentally. When that is achieved one also benefits from the extra detail available in the theoretical output. For example, the theoretical results may include interesting information about the dependence of cross sections on initial vibrational states in cases where only the initial translational energy has been experimentally varied, or they may yield product rotational distributions in cases where the experimental product-state resolution is only sufficient to distinguish vibrational structure. In other cases, theoretical rates may be calculated for systems on which no experiments have been performed. An even more dramatic example is the ability of theory to provide opacity functions, which are transition probabilities as functions of impact parameter. These functions are absolutely unattainable experimentally. Of course, for many or even most systems of interest the available potential energy surfaces and those that may be calculated with state-of-the-art methods and basis sets are either not of chemical accuracy or are at least not of demonstrated

reliability. Sometimes additional errors are also introduced by the dynamics calculations. Thus the field of ab initio potential energy surfaces combined with dynamics calculations is currently in a critical infancy stage involving the testing of various methodologies and attempts to demonstrate for a few prototype systems what can and cannot be accomplished.

In our own research group, we have used ab initio potential energy surfaces to perform dynamics calculations (i.e., calculations of cross sections, rate constants, transition probabilities, or dynamical attributes such as threshold energies) on several systems including the chemical reactions $\text{H} + \text{p-H}_2 \rightarrow \text{o-H}_2 + \text{H}$ or 3H [1-19], $\text{OH} + \text{H}_2 \rightarrow \text{H}_2\text{O} + \text{H}$ [8,20-22], $^{35}\text{Cl} + \text{H}^{37}\text{Cl} \rightarrow \text{H}^{35}\text{Cl} + ^{37}\text{Cl}$ [23], $\text{O} + \text{OH} \rightarrow \text{O}_2 + \text{H}$ or HO_2 [24], $\text{O} + \text{H}_2 \rightarrow \text{OH} + \text{H}$ [25], $\text{F} + \text{H}_2 \rightarrow \text{HF} + \text{H}$ [26,27] $\text{H} + \text{H}'\text{F} \rightarrow \text{HF} + \text{H}'$ [26], $\text{H} + \text{H}'\text{Cl} \rightarrow \text{HCl} + \text{H}'$ [28] (including in most cases additional isotopic analogs), and energy-transfer processes in collisions of H with H_2 [29,30], He with HD [31], He with I_2 [32,33], and HF with HF [34]. In keeping with the theme of the present symposium, namely the state of the art of electronic structure calculations and the comparison of results obtained from such calculations to experiment, we present here a review of a selected subset of systems recently studied in our group for which the potential energy surfaces are, in some sense, state-of-the-art. In particular, we discuss $\text{F} + \text{H}_2$, $\text{H} + \text{H}'\text{F}$, $\text{H} + \text{H}'\text{Cl}$, $\text{H} + \text{CH}_3$, $\text{He} + \text{I}_2$, and $\text{HF} + \text{HF}$ collisions, as well as additional isotopic analogs in some cases. In all these cases we performed at least some electronic structure calculations [26,28,33-37] in our own group; but for $\text{HF} + \text{HF}$ our dynamics calculations are based entirely on a surface calculated by Binkley and fit by Redmon [38]. It is becoming increasingly clear that, when electronic structure calculations and dynamics calculations are not performed in the same group, at least a close collaboration of potential-energy-surface builders with potential-energy-surface users is highly desirable.

The methods used in the electronic structure calculations that were performed in our group can be divided into two categories:

1) methods employing a single reference (SR) configuration and
2) methods employing multiple (two or more) reference (MR) configurations. If the system under investigation can be described reasonably well by a single-configuration wavefunction, as is the case for the H-F-H' system even at its saddlepoint [26], then SR methods are employed. In particular the orbitals are optimized using the spin-restricted Hartree-Fock self-consistent-field method [39], which will be abbreviated RHF, and the correlation energy is calculated from a configuration interaction (CI) wavefunction that includes all single and double (SD) excitations from one reference configuration [40]; such a CI calculation will be abbreviated SR-CISD, and the combination of methods will be denoted RHF/SR-CISD. When more than one configuration is too important to be considered as a perturbation, e.g., in the dissociation of CH₄ [35], then MR methods are used. In the MR methods, the orbitals are optimized with respect to the set of reference configurations in a multi-configuration self-consistent-field (MCSCF) calculation [41-44], and the CI wavefunction consists of all single and double excitations from the same set of reference configurations. The resulting wavefunction will be denoted as MCSCF/MR-CISD. A special case occurs when the set of reference configurations consists of all spin- and symmetry-allowed occupations of a number of electrons in a pre-specified manifold of orbitals, called the active orbitals. In this case the reference configurations are said to form a complete-active-space (CAS) [41] set, and the resulting wavefunction will be denoted CASSCF/MR-CISD. These methods, RHF/SR-CISD, MCSCF/MR-CISD, and CASSCF/MR-CISD, were used as implemented in the COLUMBUS [45-48] electronic structure codes.

Although the present chapter is written in the form of a review, it does include some new work (both electronic structure and dynamics calculations) not described elsewhere. Since the present chapter is devoted primarily to our own work, we conclude this introduction by giving a few references to recent reviews from which other recent work along similar lines may be traced [49-52].

2. CHEMICAL REACTIONS

2.1 $H + FH' \rightarrow HF + H'$ and $H + ClH' \rightarrow HCl + H'$: ab initio predictions of high barriers

Several recent experimental [53-55] and theoretical [56-60] investigations have shed light on the potential energy surface of the $H + FH' \rightarrow HF + H'$ reaction, especially in the region of the H-F-H' saddlepoint. These investigations have indicated that the barrier height for this thermoneutral exchange reaction is significantly higher than that predicted by many of the standard extended-LEPS-type [61] potential energy surfaces, including the Muckerman surface no. 5 [62] (M5), which is widely used for the alternative reaction channel $F + HH' \rightarrow HF + H'$, but which has a barrier height for the exchange channel of only 1.8 kcal/mol [63]. In comparison, Bott has concluded that the activation energy, E_a , must be greater than 19 kcal/mol to be consistent with rate constants measured in a shock tube study [54]. Furthermore, by monitoring the chemiluminescence and mass spectrum of the products from the reaction of vibrationally excited HF molecules with D, Bartoszek et al. [55] have obtained a set of bounds placing the effective threshold energy for the exchange channel in the range 41-52 kcal/mol. Ab initio values of the barrier height derived from calculations at the collinear H-F-H' saddlepoint geometry are presented in the first six rows of Table 1 and these values, which are in the range 44-49 kcal/mol, are in excellent agreement with the bounds of Bartoszek et al. [55]. Wadt and Winter [58] have also calculated the unconstrained H-F-H' saddlepoint and their result is given in the last row of Table 1; the energy lowering due to relaxing the collinear constraint is only about 1 kcal/mol. In further investigations of the bend potential of the H-F-H' saddlepoint, they found, for $R(H-F) = 2.154 a_0$, that the potential energy for C_{2v} H-F-H' is almost constant when the bond angle $\theta_{HFH'}$ is varied from 180 to 120 deg. Thus, the remainder of this section will only discuss the collinear saddlepoint.

We performed several large-scale configuration interaction

Table 1. Summary of ab initio energies E and classical barrier heights V^\ddagger for H - F - H'.

R(H-F) ^a (a ₀)	E(E _h)	V [‡] (kcal/mol)	Source
Collinear saddle point			
R(HF)(a ₀)			
2.154	...	49.0	Bender <u>et al.</u> [56]
2.160	-100.7750	44.9	Botschwina and Meyer [57]
2.154	-100.6583	48.1	Wadt and Winter [58]
2.154	...	47.7	Voter and Goddard [59]
2.230	-100.6622	48.8	Dunning [60]
2.154	-100.7328	44.4	Table 2 and Ref. [26]
Unconstrained saddle point ^b			
2.041	-100.6602	46.9	Wadt and Winter [58]

^a R(H-F) = R(F-H')

^b θ , the H-F-H angle, is 106 deg.

calculations on FH₂ to calibrate two new analytic potential energy surfaces for this system. These new FH₂ surfaces, called surfaces nos. 4 and 5, are based on ab initio calculations for the H-F-H' saddlepoint region and experimental data [64-66] for the F-H-H' saddlepoint region, and they have also been calibrated in the F-H...H exit channel region, with surface no. 4 based in that region on results from additional ab initio calculations [26] that will be discussed in the next section, and surface no. 5 further adjusted semiempirically.

In order to determine which ab initio approach, SR or MR, is needed to characterize the H-F-H' saddle point region accurately, a preliminary set of calculations was performed using both methods with a 6-311G** basis set [26]. A comparison of the results from these calculations indicated that this saddlepoint region is

described well by a single dominant configuration and thus the RHF/SR-CISD method was used in the larger-scale calculations. In all calculations, the F 1s orbital was constrained to be doubly occupied and a partial Hartree-Fock interacting space limitation [67] was imposed on the configuration space. Also we calculated a correction for the effect of unlinked quadruple excitations [40] using the standard Davidson correction [68], namely,

$$\Delta E_Q = \Delta E_{SD}(1 - c_0^2) \quad (1)$$

where ΔE_Q is the estimate of the energy contribution from the unlinked quadruple excitations, ΔE_{SD} is the correlation energy from the RHF/SR-CISD calculation, and c_0 is the coefficient of the reference configuration in the RHF/SR-CISD wavefunction. Results including the Davidson quadruples correction will be denoted RHF/SR-CISD + Q.

In the final calculations used in determining the H-F-H' barrier height, we employed a large (10s6p4d/5s3p)/[8s5p4d/4s3p] contracted gaussian basis set. This basis set was adapted from the smaller basis of Botschwina and Meyer [57] by addition of diffuse p subshells to the F and H atoms (with exponential parameters of 0.0796 and 0.120, respectively) and by replacement of the two d subshells on F with four (with exponential parameters of 3.0, 1.09, 0.40, and 0.14). In this basis set, the SCF/SR-CISD wavefunction in C_{2v} symmetry includes 22760 configurations.

The results of our calculations [26] for two geometries in the vicinity of the H-F-H' saddlepoint are summarized in Table 2. The geometry given in the first row is that of the saddlepoint that was optimized by Wadt and Winter [58] using the PNO-CEPA method with a (12s8p3d1f/6s2p)/[9s6p3d1f/4s2p] gaussian basis set. The geometry given in the second row is obtained by an asymmetric stretch of the first geometry. The calculated barrier height of 44.4 kcal/mol is consistent with the high barrier obtained in the previous ab initio calculations [56-60], as shown in Table 1. The

results in Table 2 were used in the calibration of surfaces nos. 4 and 5 discussed in the next section. Using the final surface, no. 5, the shape of the H-F-H' exchange barrier may be compared to that for the very well characterized H-H-H' exchange barrier. In a recent paper Liu [69] has presented new calculations for the potential energy surface for H₃ that are believed to converge it to within about 0.1 kcal/mol of the exact surface in the 3-body interaction region. On the basis of these calculations he recommended subtracting 0.15-0.21 kcal/mol from the previous [70] H + H₂ interaction energies. In Figure 1 we compare H + HH' interaction energies, obtained by subtracting 0.15 kcal/mol (which is hardly noticeable on the scale of the plot) from the previous [70] surface, to H + FH' interaction energies calculated from surface no. 5. In both cases the interaction energy is given as a function of the asymmetric stretch coordinate. It can be seen that the two exchange barriers have quite different characters. For H-F-H', the rectilinear asymmetric stretch lowers the interaction energy to a small fraction of its transition state value before a repulsive wall is encountered, whereas for H-H-H' this is not true. The consequences of this difference for the dynamics are unknown.

Table 2. Total and interaction energies for SR-CISD calculations in the vicinity of the saddlepoint for H+FH' → HF+H'.

R(F-H')	R(F-H)	θ _{HFH'}	E(SR-CISD)	ΔE(SR-CISD) ^a	ΔE(SR-CISD+Q) ^a
(a ₀)	(a ₀)	(deg)	(E _h)	(kcal/mol)	(kcal/mol)
2.1540	2.1540	180	-100.732837	47.85	44.40
1.8540	2.4540	180	-100.756668	32.89	31.58

^a ΔE = E(H-F-H') - E(H+H'F) separated from H'F by 20 a₀.

Another exchange reaction that has received much experimental [71-80] and theoretical [57,59,60,81,82] attention is the H + ClH' → HCl + H' reaction and its isotopic analogs. The height of the H-Cl-H' transition state is not nearly as well characterized

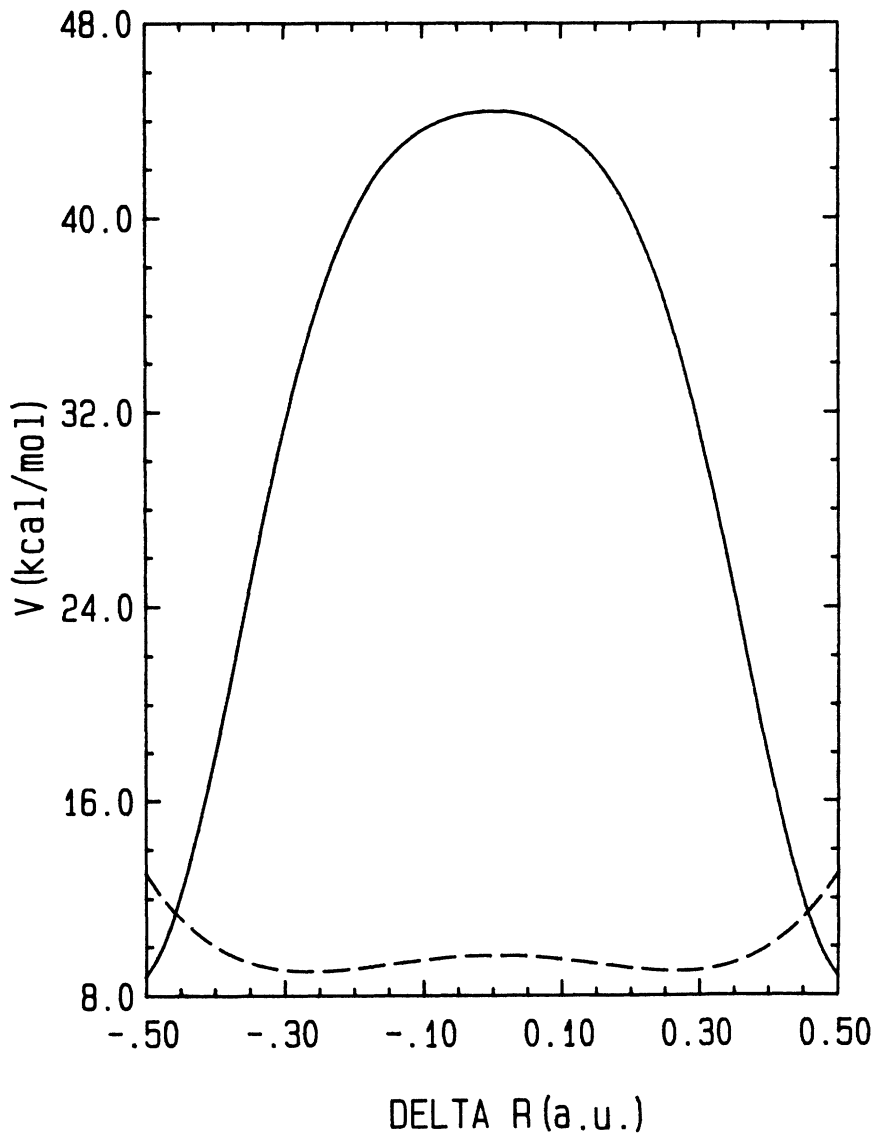


Figure 1. Exchange barrier for $H+FH'$ (solid curve) and $H+HH'$ (dashed curve) along the asymmetric stretch coordinate. The geometries are defined by $R(H-X) = R^\ddagger(H-X) + \Delta R$, $R(X-H') = R^\ddagger(H-X) - \Delta R$, and $R(H-H') = R(H-X) + R(X-H')$, where $R^\ddagger(H-X)$ is $2.154 a_0$ for $X=F$ and $1.757 a_0$ for $X=H$. The ordinate is interaction energy, defined as $\Delta E = E(HXH') - E(H + XH')$.

as is that of H-F-H'. The results from several relevant experimental measurements are mutually inconsistent [71-81]. For example, Klein and Veltman [75] have measured the branching ratios for the D(H) + HCl(DCl) system using a discharge flow reactor with a quadrupole mass spectrometer for product detection. Combining their value for the difference in activation energies of the abstraction and exchange reactions with a recent value of 3.2 kcal/mol [79] for E_a of the abstraction reaction, one obtains a value of $E_a = 2.1$ kcal/mol for the exchange reaction. Endo and Glass [74], employing a discharge flow reactor with EPR detection, obtained $E_a > 4$ kcal/mol. A more direct experiment, by Miller and Gordon [79], which utilized laser photolysis to generate the D atoms and resonance fluorescence to monitor the concentration of the H, D, and Cl atoms present, yielded no observable exchange at 325K, and this put an approximate lower limit of 7 kcal/mol on E_a .

McDonald and Herschbach [73] observed the exchange reaction $D + HCl \rightarrow DCl + H$ in a molecular beam apparatus with a nearly Maxwellian speed distribution and a mean relative transitional energy of 9 kcal/mol. For such a distribution, 13% of the collisions have a collision energy greater than 20 kcal/mol and 10% have a collision energy in excess of 22 kcal/mol. Thus, as pointed out by Miller and Gordon [79], this experiment only places an approximate upper bound of about 20-22 kcal/mol on the threshold energy and hence presumably an approximate bound of about the same magnitude on the barrier height. Toennies and coworkers, in a later study, at first reported a confirmation of the McDonald-Herschbach experiment, and obtained an apparent activation energy of 20 ± 6 kcal/mol [77]. Later, however, a more refined and extensive experimental study [78] indicated that the observed H atoms did not arise from the exchange reaction as originally assumed. As a result these experiments do not appear to give any information about the threshold energy for exchange.

Very recently, Wight et al. [80] have observed infrared fluorescence from vibrationally and rotationally excited HCl pro-

duced by the reaction of DCl with H atoms with 22 kcal/mol translational energy. This places an upper bound of 22 kcal/mol on the exchange threshold. The bound could not be improved because no precursor molecule is known for which excimer laser photolysis yields H atoms with a lower translational energy.

If we assume that activation energy, threshold energy, and classical barrier height are the same within about 2 kcal/mol, then the two most recent experiments [79,80] may be combined to place the exchange barrier in the range 5-24 kcal/mol, whereas the Wood [72] and Klein-Veltman [75] studies imply lower barriers.

Semiempirical LEPS-type potential energy surfaces that have been calibrated for the $\text{Cl} + \text{HH}' \rightarrow \text{HCl} + \text{H}'$ reaction have a shallow well on the exchange reaction path [83]. Ab initio calculations of the barrier height for the exchange reaction have not yet completely converged, but they definitely yield a more consistent picture than the experiments or the semiempirical calculations. Firstly, they all predict a barrier rather than a well for symmetric H-Cl-H' geometries. Botschwina and Meyer [57] have performed PNO-CEPA calculations on this system using a large (13s10p3d1f/6s2p)/[9s7p3d1f/4s2p] basis set and find a barrier of 22.1 kcal/mol. However, they estimate the value of the true barrier height to lie between 10 and 15 kcal/mol based upon the use of a semiempirical methods [57,84] for correcting the calculated value for errors in the correlation energy arising from the use of a truncated basis set and a truncated CI expansion. Dunning [82] has investigated this system by optimizing the geometry of the saddlepoint using the POL-CI method in a (12s9p2d/5s1p)/[4s4p2d/3s1p] basis set. A barrier height of 25.3 kcal/mol was obtained from a GVB+1+2 calculation using this basis set and geometry. Based upon an estimate of the error in the calculated Cl-H-H' barrier height, Dunning concludes that the true H-Cl-H' barrier height lies in the range 14.1-21.7 kcal/mol. Using the generalized resonating valence bond method with a valence double zeta plus polarization basis set, Voter and Goddard [59] have calculated a barrier of 25.5 kcal/mol at Dunning's collinear geometry. Recently, Dunning has re-examined

the H-Cl-H' barrier height using the same GVB+1+2 method but with a smaller (11s7p1d/4s2p)/[4s3p1d/2s1p] basis, and he obtained a barrier of 23.5 kcal/mol [60]. Thus all previous ab initio calculations predict a high barrier height in the range of 21-26 kcal/mol, although in some cases lower values in the range 10-22 kcal/mol have been estimated by considering various errors in the calculations.

We have recently begun an investigation of H-Cl-H' barrier region using the CASSCF/MR-CISD method [28]. The reference space consists of 28 configurations constructed from the 9 valence electrons occupying the 6 valence orbitals. We have used Botschwina and Meyer's larger, (13s10p3d1f)/[9s7p3d1f], chlorine basis, and we augmented their smaller, (5s2p)/[4s2p], hydrogen basis with a d subshell with an exponential parameter of 1.67. The largest calculation performed on bent C_{2v} H-Cl-H' included 323908 configurations. Using the PNO-CEPA collinear saddlepoint geometry of Botschwina and Meyer [57], for which $R(\text{H-Cl}) = R(\text{Cl-H}') = 2.8384 a_0$, we have obtained a total energy of $-460.787253 E_h$ and a barrier height of 20.9 kcal/mol. Interestingly, an RHF/SR-CISD+Q calculation with the same one-electron basis yields a barrier height of 20.7 kcal/mol indicating that the multi-reference CISD calculation includes the most important geometry-dependent quadrupole excitations from the dominant configuration. These values, 20.7 - 20.9 kcal/mol, are slightly lower than the uncorrected values reported earlier [57,59,60,82] and are within the upper bound that may be estimated from the experiment of Wight et al [80].

In summary, ab initio calculations without semiempirical corrections yield high barrier heights of about 21 kcal/mol or greater. Although this high a value does not contradict the results from recent experiments, further work needs to be done on this system to make the predictions more definitive.

2.2 Entrance- and exit-channel barriers in the $F + H_2 \rightarrow HF + H$ reaction and isotopic analogs

The $F + H_2$ reaction has been widely studied both experimentally and theoretically, largely because of its importance in pumping the HF chemical laser [85-87]. Currently, interest has been heightened by theoretical and experimental evidence of reactive resonances for this system [64-66,88,89]. Most of the early experiments concentrated on measurements of product state distributions [90-96] and recently there have been precise determinations of the room temperature thermal rate constants [97,98] and measurements of detailed vibrational-state-resolved differential cross sections [64-66, 99].

Although ab initio potential energy data has been available for the $F + H_2$ reaction for over 12 years [100-102], most dynamical studies have used the semiempirical surface no. 5 of Muckerman (M5) [62] because of its convenience and because a fit to the available ab initio results is not definitely more reliable. The M5 surface is an extended LEPS form in which the two Sato parameters were adjusted so that: (a) the room temperature activation energy computed using conventional transition state theory reproduced the experimental value [103] accepted at that time of 1.7 kcal/mol; and (b) the average vibrational energy of the product HF molecule computed using quasiclassical trajectories [62] agreed with experiments [91] for the fraction of the exothermicity deposited in product vibration under thermal conditions.

As experiments on the $F + H_2$ reaction and its isotopic analogs have become more refined and have offered more precise and detailed information, comparison between these data and dynamical calculations on the M5 surface have indicated deficiencies in this surface. First, two recent experiments [97,98] give an activation energy for the $F + H_2$ reaction of 0.9 to 1.1 kcal/mol rather than the 1.7 kcal/mol used to adjust the M5 surface. Secondly, cross sections for production of $HF(v=3)$ and $DF(v=4)$ (v denotes vibrational quantum number) computed using approximate quantal methods [89] on the M5 sur-

face are not appreciable until almost 2 kcal/mol above the energetic threshold. These "delayed thresholds" are not observed experimentally [64-66]. In Figure 2a the heights of the vibrationally adiabatic potential curves are given at critical points of the potential energy surface for the $F + H_2$ and $F + D_2$ reactions. In each case the zero of energy is taken as the infinitely separated reactants in their ground vibrational state. In this diagram one sees that $HF(v=3)$ and $DF(v=4)$ both have energies relatively close to ground-state reactants, hence the delayed threshold effect is seen at energies just above the overall reaction threshold.

Direct comparison with ab initio data also indicates errors in the M5 surface. The potential energy change as F-H-H is bent from collinear geometries in the entrance channel is much steeper for the M5 surface than seen in ab initio calculations [100]. Also, as discussed in the previous section, the H-F-H' exchange barrier on the M5 surface is much lower than indicated by ab initio calculations [26,56-60].

We have used variational transition state theory (VTST) methods [2,6,8,104-108] first to learn which regions of the surface are most critical for determining thermal rate data (including activation energies) and are responsible for the magnitudes or absence of delayed thresholds, and, second, to characterize those portions of the potential energy surface. In VTST the dynamical bottleneck to chemical reaction at low temperatures is located at the maximum in the ground-state adiabatic potential curve [6]. The adiabatic potential curve is given by

$$V_a(\alpha, s) = V_{MEP}(s) + \epsilon_{int}(\alpha, s) \quad (2)$$

where s is the distance along the minimum energy path (MEP), α and $\epsilon_{int}(\alpha, s)$ are respectively the set of quantum numbers and the internal energy for the degrees of freedom normal to the reaction path, and $V_{MEP}(s)$ is the potential along the MEP. For the $F + H_2$ reaction the barrier on the entrance-channel portion of the ground-state adiabatic potential curve controls the thermal rates and

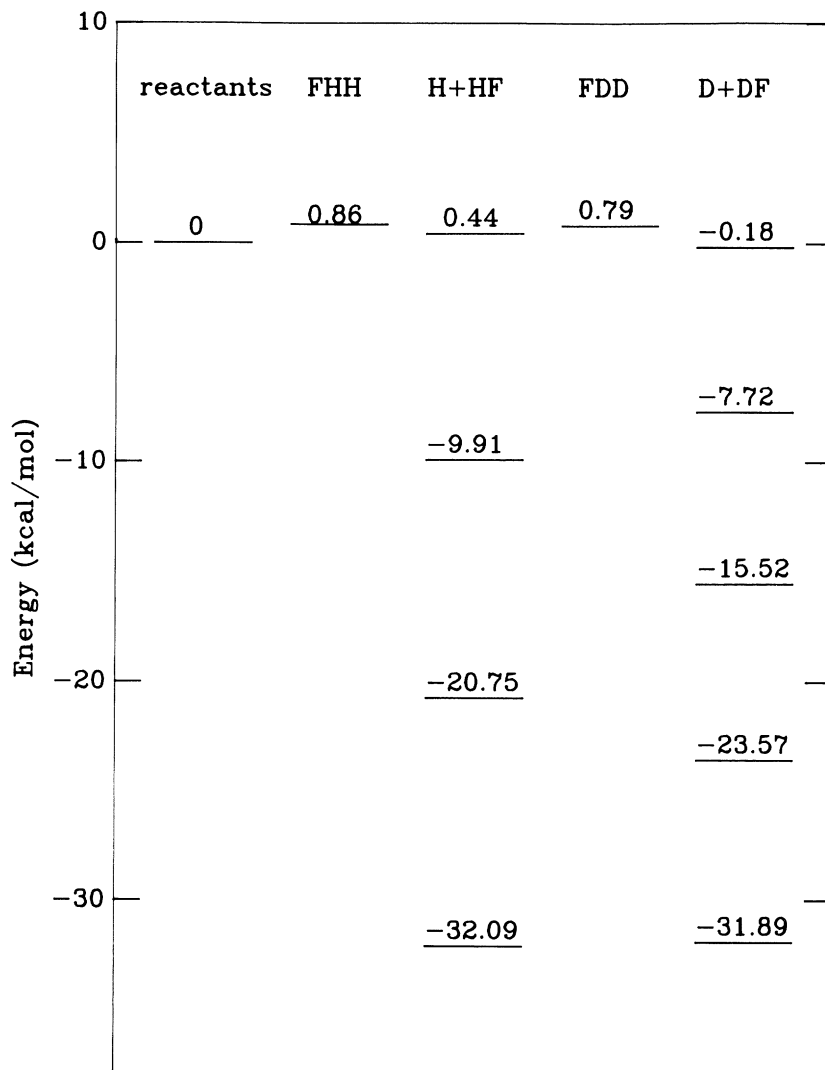


Figure 2a. Energetics of the three-dimensional $F + H_2 \rightarrow H + HF$ and $F + D_2 \rightarrow D + DF$ systems. The energies for each system are relative to reactants in the ground vibrational state for that system; this zero of energy is shown in the first column. The vibrationally adiabatic energies for two saddlepoints, FHH and FDD, are also shown in the figure. The third and fifth columns show the vibrational levels of the products, namely the ground state and the first three excited vibrational states for HF and the ground state and the first four excited vibrational states for DF.

activation energies. This barrier is below the energetic threshold for production of the excited species HF($v=3$) on the M5 surface. Thus the entrance-channel barrier does not determine the threshold for production of this excited state product. We have compared [109] barriers on exit-channel portions of excited-state adiabatic potential curves with thresholds for production of excited states obtained from an approximate quantal method (the bend-corrected rotating linear model or BCRLM) [110], and we found good agreement when the stretch vibrational energy levels in Eqn. (2) are computed using the WKB approximation [108]. The exit-channel barrier determines the delayed threshold when it is higher than both the energetic threshold and the entrance-channel barrier. In summary then, if a surface is to be accurate both for overall rate constants and for state-specific production distributions, it is important that the surface be accurate in two regions, namely the region near the maximum of $V_a(\alpha = \text{ground state}, s)$ in the entrance channel and also the region where $V_a(\alpha, s)$ has its maxima for HF($v=3$) and DF($v=4$) in the exit channel.

One approach to fitting these critical portions of the potential energy surface more accurately is to vary the potential in these regions until the results of dynamical calculations agree with the experimental results. Alternatively, the potential in a critical region can be improved by fitting to accurate ab initio potential data. Although the latter approach is more pertinent to the theme of the present discussion, it was used only for the exit channel. First we discuss an attempt [111] we made to use the former approach to reoptimize an extended LEPS surface in the entrance channel region in a manner similar to that used by Muckerman [62]. As the first step, the Sato parameters were adjusted (i) so that the activation energy computed by canonical variational theory [2,8,104-106,108] with a small-curvature semiclassical adiabatic ground state tunneling correction [8,107] (CVT/SCSAG) reproduces the experimental activation energy [97,98] for the $F + D_2$ reaction in the temperature range 295-373 K; and (ii)

so that a model prediction of the average vibrational energy of the DF product agrees with experiment. The reoptimized LEPS potential was used for the collinear part of a new surface and the non-collinear part was refit using ab initio data [100]. The fit was accomplished by replacing the constant HF Sato parameter by one that is a function of the angle between the H₂-to-F vector and the HH axis. Some thermal rate constants for the F + H₂ and F + D₂ reactions computed using the CVT/SCSAG method on surfaces M5 and the new surface, called no. 2, are presented in Table 3 and are compared with experiment [97,98,112]. Surface no. 2 is seen to be in much better agreement than surface M5 with these experiments for both reactions; however, it still predicts significant, and presumably erroneous, delayed thresholds for HF(v=3) and DF(v=4).

Table 3. Thermal rate constants (units of cm³ molecule⁻¹s⁻¹) for the F + H₂ and F+D₂ reactions

T(K)	Surface	CVT/SCSAG			experiment
		M5	No. 2	No. 5	
200	F + H ₂	1.1(-12) ^a	8.7(-12)	1.3(-11)	1.1(-11) ^b
300		3.9(-12)	1.7(-11)	2.5(-11)	2.8(-11) ^b
600		1.5(-11)	3.7(-11)	5.7(-11)	7.3(-11) ^b
200	F + D ₂	7.9(-13)	5.5(-12)	7.1(-12)	5.7(-12) ^c
300		2.5(-12)	1.1(-11)	1.4(-11)	1.4(-11) ^{c,d}
600		9.4(-12)	2.3(-11)	3.3(-11)	3.9(-11) ^d

^a Numbers in parenthesis are powers of ten.

^b Preferred values from review of reference 112.

^c Reference 97.

^d Reference 98.

To try to learn the nature of the potential energy surface in the region responsible for the delayed thresholds, ab initio electronic structure calculations were performed for geometries in the product channel [26]. The details of these calculations have

been described in Ref. 26 and Section 2.1. In the product region an SR approach might be expected to be adequate because FH...H is similar to Ne...H, and one electronic configuration dominates. At four geometries, we performed both RHF and CASSCF calculations to test this assumption, and it was confirmed. Thus the SR approach was used for the calibration. Using surface no. 2 as a starting point, the ab initio data was used to fit the HH Sato parameter to a function of the HH distance and the bend angle. The fit was tailored to change the potential in the entrance channel as little as possible. The resulting surface is called surface no. 4. In Figure 2b, we compare the entrance- and exit-channel adiabatic potential curves for the $F + H_2$ reaction for the M5 and no. 4 surfaces. By using ab initio data to refit the exit-channel region of the potential energy surface, the exit-channel barrier for the production of $HF(v=3)$ has been reduced from 2.5 kcal/mol above the energetic threshold on surface M5 to 1.0 kcal/mol above this energetic threshold, as shown in Figure 2b.

Although surface no. 4 gives a much better description of the state-specific threshold energies than surface M5, the predicted highest-product-state thresholds are still larger than their experimental counterparts, which appear not to be delayed at all above the energetic thresholds. Furthermore, CASSCF/MR-CISD ab initio calculations [26] indicate that improving the reference space and the basis set (by adding an f shell and by changing the exponents on the polarization functions), which increases the number of configurations to 218512, still decreases the potential energies (relative to the $HF + H$ asymptote), but the decrease is very small as the basis is increased. We were able to lower the ab initio surface in the critical region by only 0.2-0.5 kcal/mol, and these small changes are not large enough to account for the discrepancy with experiment. Thus we decided to employ an empirical modification to surface no. 4 to lower the exit-channel barrier even further. The exit-channel region of surface no. 4 was readjusted to fit the threshold energy for the $F + HD \rightarrow HF(v=3) + D$ reaction,

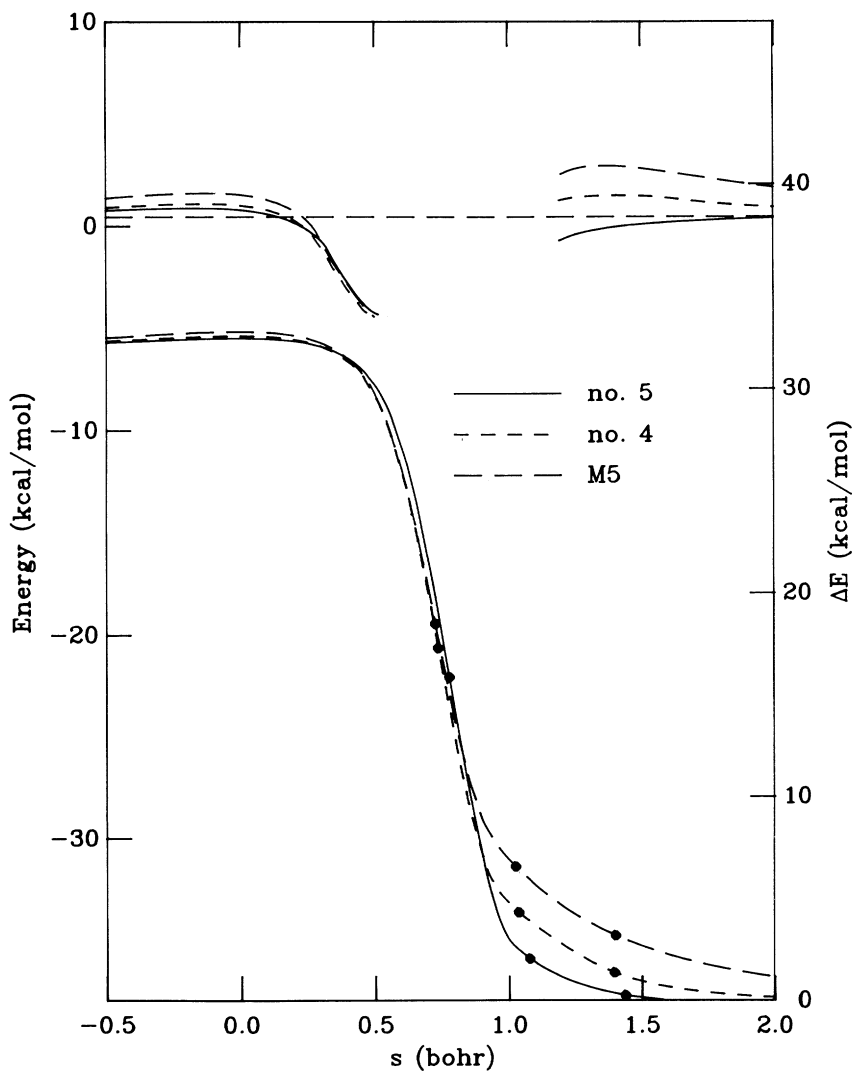


Figure 2b. The classical (V_{MEP}) and vibrationally adiabatic (V_a) energy curves along the MEP for three-dimensional $F + H_2(v=0) \rightarrow HF(v=3) + H$ on surfaces M5, no. 4, and no. 5. The abscissa gives the distance along the MEP with $s=0$ corresponding to the saddlepoint. The upper two sets of curves show the vibrationally adiabatic entrance-channel ($v=0$) and exit-channel ($v=3$) barriers for these surfaces. The lower curves are the potential energy along the MEP with the circles corresponding to H-H bond lengths of $2.0 a_0$, $2.5 a_0$, and $3.0 a_0$. The left-side energy scale is the same as for Figure 2a and the right-side scale is the same as for Figure 1. The dashed horizontal line is the energetic threshold for $HF(v=3)$.

which has the most accurately determined experimental threshold energy [64-66]. The entrance- and exit-channel barriers for the $F + H_2$ reaction on this final surface, no. 5, are also shown in Figure 2b. Surface no. 5 exhibits no delayed threshold for either the $F + H_2 \rightarrow HF(v=3) + H$ or the $F + D_2 \rightarrow DF(v=4) + D$ reaction. The thermal rate constants on surface no. 5 are also shown in Table 3. The entrance-channel region for surface no. 5 is very similar to that for surfaces nos. 2 and 4 and the thermal rate constants do not differ greatly on the three surfaces.

Using a combination of ab initio and experimental data a potential energy surface has been constructed which is consistent with the most modern thermal rate data and with the experimental threshold energies for production of vibrationally excited products, as well as with ab initio calculations on the H-F-H' exchange barrier. It will be interesting to see the effect surface no. 5 will have upon accurate dynamical calculations of detailed quantities such as differential cross sections and the prediction of reactive resonances.

2.3 $CH_3 + H \rightarrow CH_4$

The dissociation of CH_4 presents an interesting system as the starting point for the development of polyatomic potential energy surfaces. This system can serve as a prototype for both radical recombination and polyatomic dissociation potentials for more complicated organic systems. In a recent study, Duchovic and Hase [113] have demonstrated the sensitivity of calculated rate constants for the recombination reaction $H + CH_3 \rightarrow CH_4$ to the shape of the potential curve in the region where $R(C-H)$ is 3.5-6.0 a_0 (about two to three times the equilibrium value of 2.052 a_0 in methane). In this work, two different potential curves along the reaction coordinate, which corresponds to the making of a C-H bond in methane, were obtained by fitting previous calculations [114] carried out using Møller-Plesset (Many-Body) fourth order (MP4) perturbation theory with 6-31G** basis set to two different functional

forms, and these curves were both used to calculate rate constants. The first functional form used was a standard Morse function, and the second form was a "stiff" Morse function in which the constant range parameter was replaced by a polynomial in $R(\text{C-H})$. Figure 3 shows that the main difference in these two potential curves is in the region $3.5 a_0 \leq R(\text{C-H}) \leq 6.0 a_0$ where the stiff Morse function, which more closely fits the MP4 results, is less attractive than the standard Morse function. Thermal rate constants for the $\text{H} + \text{CH}_3$ association reaction at 300 K were calculated by running Monte Carlo classical trajectories on two potential energy surfaces [115] that differ only in the form of the potential curve along the reaction coordinate. It was found that the surface with the stiff Morse function yielded a rate constant ten times smaller than the rate constant from the surface with the standard Morse function, while the experimental [116] rate constant is near the geometric mean of these two values. This shows that the potential in the region $3.5 a_0 \leq R(\text{C-H}) \leq 6.0 a_0$ plays a very large role in the dynamics of this system.

In a recent study [117] of the symmetric dissociation of H_2O , it was shown that the CASSCF/MR-CISD method gives a more balanced treatment of the correlation energy along the dissociation coordinate than the MP4 method and yields potential energy curves which are more parallel to the true potential. We expect that this may be true for the potential along any dissociation coordinate leading to fragments with free valence. Hence, in order to check the large deviation of the MP4 results [114] from the standard Morse model along the dissociation coordinate of methane, we have investigated [35] this potential curve using the CASSCF/MR-CISD method. For these calculations, we employed a large 6-311++G(df,p) basis set which includes both diffuse and polarization functions on both C and H. CASSCF/MR-CISD calculations, with 63608 configurations, were performed at the same geometries as the MP4 calculations of Duchovic *et al.* [114] and the results are shown in Figure 3.

In the region where $R(\text{C-H})$ is between 3.5 and $6.0 a_0$ our

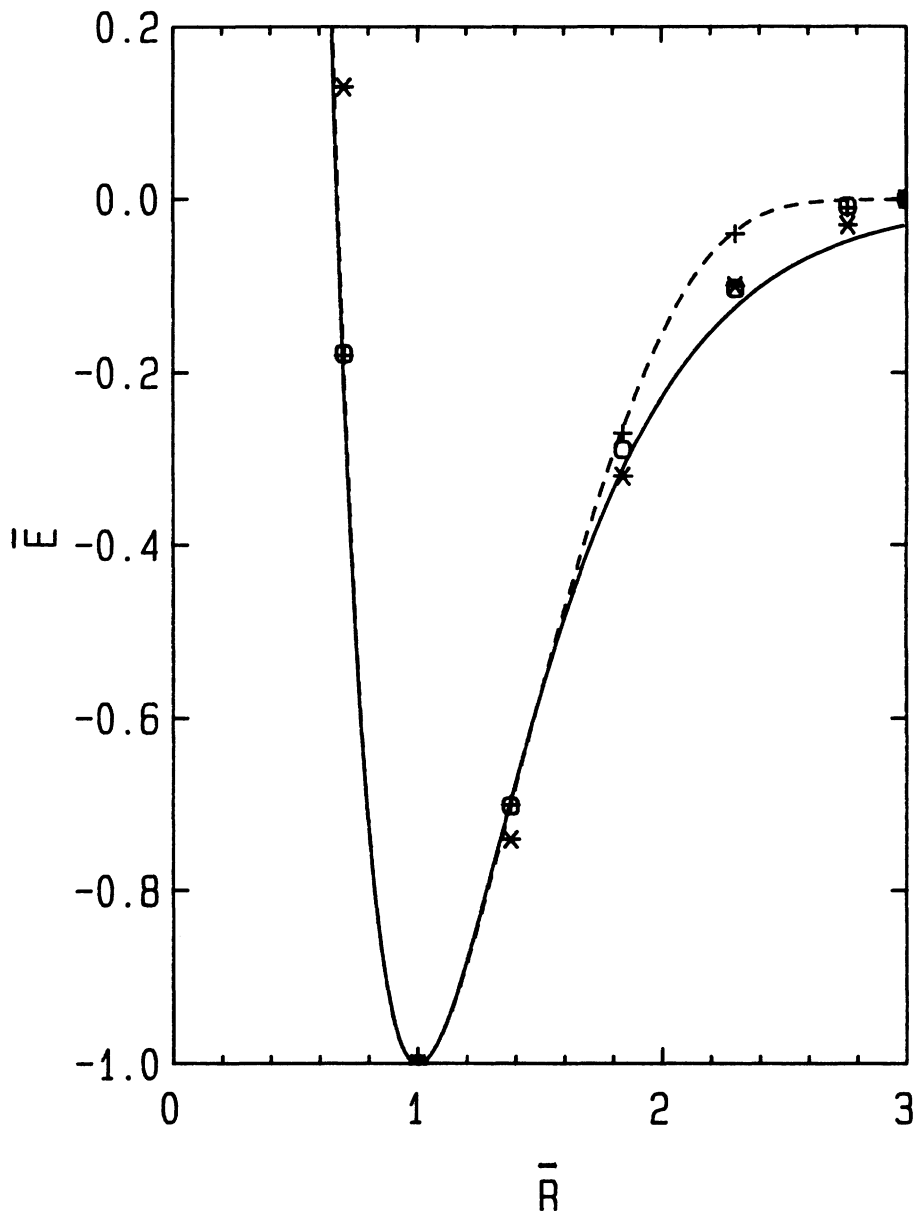


Figure 3. Potential in reduced units, $\bar{E} = [E(R(\text{C-H})) - E(\infty)]/D$, as a function of reduced C-H stretch coordinate, $\bar{R} = R(\text{C-H})/R_e$, in CH_4 : +, MP4 results from Ref. 114; -, standard Morse function based on MP4 results; ---, stiff Morse function based on MP4 results; *, Padé approximant results from Ref. 114; □, CASSCF/MR-CISD results.

MR-CISD results lie between the stiff Morse potential function, corresponding to the MP4 data, and the standard Morse potential function. Thus, presumably, a calculation of the thermal rate constant at 300 K using a functional fit of the CASSCF/MR-CISD data would yield a rate constant in better agreement with the experimental value. We have found [35] that the "first-order" Lippincott function [118]

$$V = -D \exp[-\beta(R-R_e)^2/2R] \quad (3)$$

and the Varshni III function [119]

$$V = D \left[\left\{ 1 - \frac{R_e}{R} \exp[-\beta(R^2 - R_e^2)] \right\}^2 - 1 \right] \quad (4)$$

fit the CASSCF/MR-CISD results well, which should not be too surprising since, in fact, these functional forms fit the RKR curves and experimentally derived spectroscopic constants for several diatomics better than the standard Morse curve [35,118,119].

Interestingly, Halonen and Child [120,121] have quite successfully calculated stretch overtone bands using the standard Morse function with the parameters fit to the known stretching vibrational energy levels for the C-H stretch in CH₄ and its C_{3v} isotopic analogs. However, these energy levels are located in the bottom half of the well where the Morse approximation works well, as Figure 3 shows. More recently, Peyerimhoff *et al.* [122] have performed a set of RHF/MR-CISD calculations (MRD-CI in their notation) and found that a standard Morse function gives a "reasonable" fit to these ab initio results along the C-H stretch. In contrast, we find that although the potential energy curve along the reaction coordinate of the polyatomic reaction is not unlike the dissociation potential of a typical diatomic system, it is not quantitatively represented by a Morse potential.

The failure of the MP4 method, a single-reference method, in describing H₃C-H in the intermediate bonding region can be attributed to the inability of a single reference function to describe the system adequately in this region. This inadequacy is demonstrated in Table 4 where the square of the coefficient c_0 of the

dominant configuration and sum of the squares of the coefficients c_i of the reference configurations in the CASSCF/MR-CISD wavefunction are presented for each geometry. The table shows that, near equilibrium, a single configuration describes the system well, whereas at larger $R(\text{C-H})$, the dominant configuration has a much smaller coefficient. In contrast, however, the table also shows that the total contribution of all the reference configurations is almost constant at all geometries. Thus, we believe that the CASSCF/MR-CISD method treats the potential energy curve for dissociation in a more balanced way than does the MP4 method.

Duchovic *et al.* used Padé approximants [123] to estimate the contributions of higher order terms in the perturbation series, and we can now compare the CASSCF/MR-CISD results to their results. The comparison is given in Figure 3, which shows that the Padé approximant results are indeed in better agreement with the CASSCF/MR-CISD results than are the MP4 results.

Table 4. Analysis of the MR-CISD wavefunction in terms of the coefficients of the dominant configuration and the reference configurations as a function of $R(\text{C-H})$.

$R(\text{C-H})(\text{Å})$	c_0^2	$\sum_{i=0}^{10} c_i^2$
0.757	0.957	0.960
1.086	0.938	0.944
1.500	0.916	0.941
2.000	0.850	0.942
2.500	0.737	0.942
3.000	0.617	0.942
10.584	0.454	0.943

3. ENERGY TRANSFER PROCESSES

3.1 He - I₂: cross sections for vibrational excitation

The construction of potential energy surfaces which describe the interaction between two closed-shell atoms and/or molecules presents an enormous challenge to theoretical chemists. Because the interaction energy for such systems at the van der Waals mini-

num is so tiny compared to the total energy, e.g., 1 meV for HeH₂ [124] and 2.8 meV for HeI₂ [36], accurate ab initio descriptions of this region of the potential energy surface are only currently possible for the smallest systems. Meyer et al. [124] used very large basis sets and performed configuration interaction calculations which included triple excitations to describe the van der Waals well region in the four-electron HeH₂ system, but a comparable treatment for systems with more occupied orbitals still appears prohibitive.

Even if one is able to describe the various regions of a potential energy surface to a high degree of accuracy using ab initio methods, one must also be able to analytically fit the results from these calculations to a functional form which allows for the accurate determination of dynamical properties. For the HeH₂ system, Alexander and Berard [125] have investigated the sensitivity of dynamics calculations to several fits of ab initio data from Gordon and Secrest [126] and have shown that the results are quite sensitive to the analytic fit. Duff and one of the present authors [127] further examined this question and suggested that the force exerted by He in the classically allowed region on unstretched H₂ is very useful for explaining the different dynamical results obtained from the different fits.

Recently, Hall et al. [128] have reported the first measurement of the energy dependence of a vibrational-rotational excitation cross section for a collisional system that involves only uncharged species; in particular they measured energy-dependent cross sections for He-I₂ collisions in the ground electronic state. Two potential energy surfaces based on ab initio calculations have now been constructed for He-I₂ in the ground electronic state, with special emphasis on those properties of the potential energy surface that are expected to have a strong effect on vibrational excitation [33,36].

The first surface [36] constructed in our group for He-I₂ collisions is a pairwise additive (PA) approximation that is based

in part on ab initio calculations and in part on theoretical and experimental estimates of the long-range forces and the properties of the van der Waals complex. In the ab initio calculations, a non-relativistic effective core potential [129] was used to describe the core electrons of I, and the Hartree-Fock and Møller-Plesset third-order perturbation methods were employed using a triple-zeta-plus-polarization basis set. Because of the PA approximation, ab initio calculations were only required at T-shaped geometries of the He-I₂ complex. Dynamics calculations [32] based on the rotational infinite-order-sudden approximation [130,131] on this potential yielded semiquantitative agreement with the experimental vibrational excitation cross sections; however the calculations showed significantly more rotational excitation accompanying the vibrationally inelastic events. This was ascribed to incorrect anisotropy of the PA potential. Although these calculations are only in semiquantitative agreement with experiment, they did further quantify our understanding of how the dynamics are related to the potential energy surface. We observed [32,33] that it is possible to correlate the square of the force along the I₂ bond at the classical turning point with vibrational excitation probabilities. This force $F_{\text{int}}(R_{\text{tp}})$ is $-\frac{\partial V_{\text{int}}(R, r, \chi)}{\partial r} \Big|_{r=r_e, R=R_{\text{tp}}}$, where V_{int} is the interaction energy, R is the length of the vector \vec{R} connecting the center of mass of the I₂ to He, r is the length of the vector \vec{r} connecting the I atoms, χ is the angle between \vec{R} and \vec{r} , r_e is the diatomic equilibrium internuclear distance, and R_{tp} is the classical translational turning point, i.e., the root of

$$V_{\text{int}}(R, r=r_e, \chi) + \ell(\ell+1)/(2\mu R^2) - E_{\text{rel}} = 0 \quad (5)$$

where E_{rel} is the relative translational energy in the initial state, μ is the reduced mass, and ℓ is the orbital angular momentum. For notational convenience, we define the squared vibrational force product (SVFP) for a general collisional system by

$$SVFP = \left[\prod_n F_{\text{int}}^{(n)}(R_{\text{tp}}) \right]^2 \quad (6)$$

where n runs over all (one in this subsection and two in subsection 3.2) oscillators of the target and the projectile, and $F_{\text{int}}^{(n)}(R_{\text{tp}})$ is the force exerted on the n^{th} oscillator when the radial coordinate is at its turning point and the oscillators are at their equilibrium distance. Figure 4 shows that the correlation between the vibrational excitation probability and SVFP is almost linear and not strongly dependent on the potential energy surface.

Our second HeI_2 potential energy surface [33] is improved relative to the one just discussed in three ways (i) the PA assumption is removed, (ii) results from higher quality ab initio calculations, with up to 53623 configurations, are used in constructing the potential, and (iii) an improved analytic functional form is employed.

The improvements in the ab initio methods are threefold. First, a more accurate effective core potential [132], which incorporates higher-angular-momentum projectors and relativistic effects, has been employed for the core electrons of I. Second, we used the MCSCF/MR-CISD method, which has been described in Section I, rather than the single-reference Møller-Plesset perturbation method. Since two configurations are required to describe the dissociation of I_2 , the MCSCF calculation and the multi-configuration reference space include two configurations. Third, we used an improved one-electron basis [33]. The one-electron basis set consisted of a triple zeta valence set plus two p sets on He. It is both larger and better optimized than the basis used in the previous calculations. The exponential parameters for the d subshell and for the bond centered sp shell were adjusted to best describe the I_2 bond length. Although it is not clear whether a good description of the isolated diatom is necessary for calculating the interaction force, we did insure that the calculated value for r_e , equilibrium displacement, and ω_e , the harmonic stretching fre-

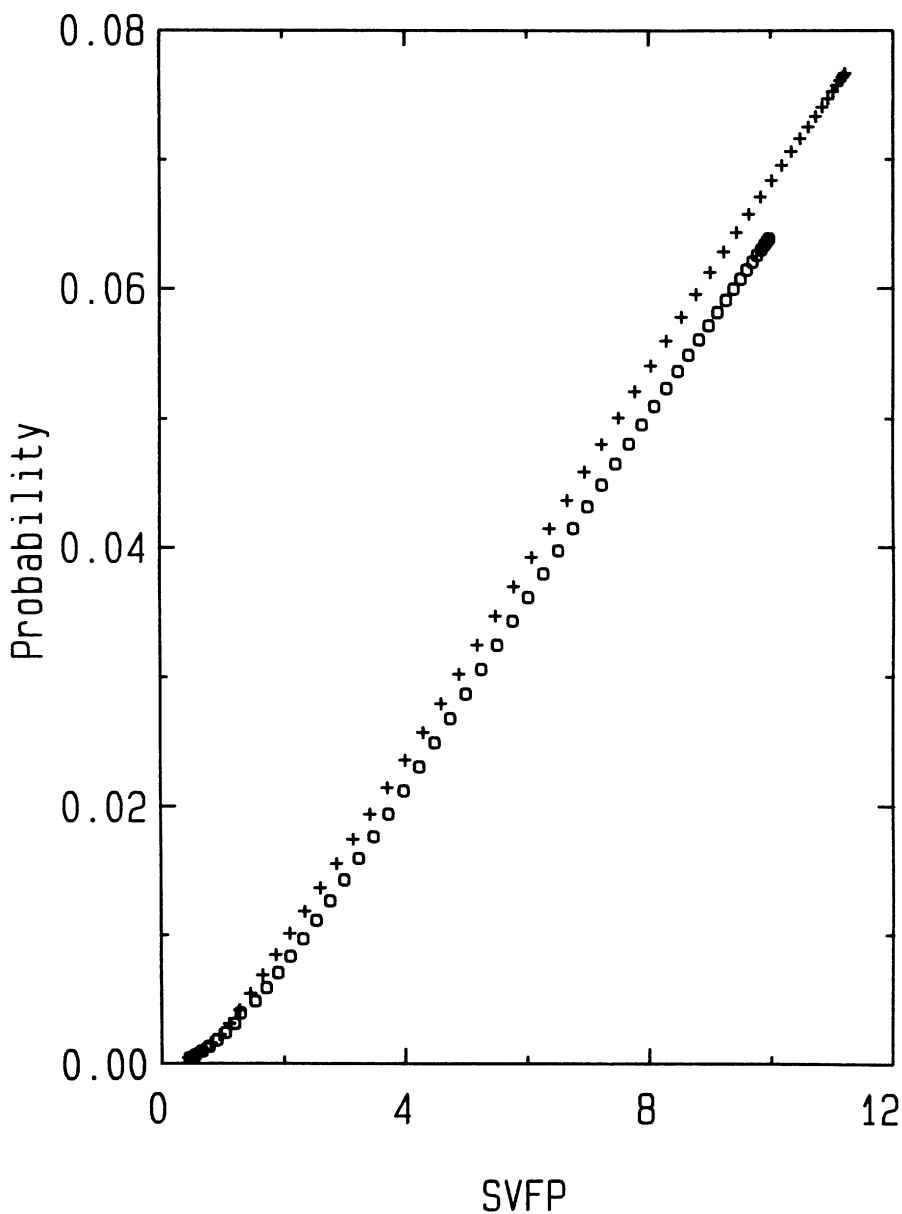


Figure 4. The probability of vibrational excitation from $v=0$ to $v=1$ in He - I₂ collisions as a function of the squared vibrational force product (SVFP) in units of 10^{-6} a.u. for $E_{rel} = 0.0867$ eV and $\chi = 0^\circ$: +, potential of Ref. 33; □, potential of Ref. 36.

quency, agree well with the experimental values. The exponential parameter for the tight p on He was adjusted to give the lowest energy for isolated He at the CISD level, and the exponential parameter for the diffuse p on He was adjusted to give a reasonable van der Waals well depth and geometry. While the prevailing experimental interpretation [133] indicates that a nonlinear geometry is more stable than a collinear one, our calculations predict that the collinear complex is more stable than the T-shaped complex by 0.09 meV. While this discrepancy is somewhat disappointing, our tests indicate that the force is better converged. In our previous study [33] we investigated the variation of the force with the He basis set and found that, when V_{int} is approximately 100 meV, the force does not vary greatly with basis changes. To test this further, in Table 5 we show the variation of the force with respect to the basis set and the treatment of electron correlation. This shows good agreement between the two CISD calculations, indicating that the calculations are well converged with respect to size of the reference space. Although Clary [134] has treated vibrational energy transfer processes for atom-polyatomic molecule collisions using small-basis-set RHF calculations, Table 5 shows that it is very important that we include polarization functions and correlation effects when estimating the force.

Table 5. Variation of the interaction energy V_{int} , and the force on the I_2 bond, F_{int} , for T-shaped HeI_2 as a function calculation method ^{a,b}.

$R(a_0)$	RHF ^c		RHF ^d		MCSCF ^d		RHF/SR-CISD ^d		MCSCF/MR-CISD ^d	
	V_{int}	F_{int}	V_{int}	F_{int}	V_{int}	F_{int}	V_{int}	F_{int}	V_{int}	F_{int}
4.0	775	215	724	184	723	191	633	170	631	174
5.0	163	24	159	21.4	159	22.7	118	16.6	118	17.3
6.0	32	-0.1	29	-1.7	29	-1.3	12	-3.3	12	-3.0
7.0	6	-1.0	5	-1.4	5	-1.2	-2	-1.8	-2	-1.7

^a V_{int} , given in meV, and F_{int} , given in meV/ a_0 , are both evaluated at $\chi=90^\circ$ and $r=5.054$ a.u., which is r_e for the MCSCF/MR-CISD calculations.

Table 5 (cont.)

-
- ^b For $\chi = 90^\circ$ and each indicated R, F_{int} is obtained by calculating V_{int} at $r=4.854$, 5.054 and $5.254 a_0$, fitting it to a parabola, and analytically evaluating the derivative at $r=5.054 a_0$.
- ^c Triple zeta basis on I and quadruple zeta basis on He without any bond-centered functions and polarization functions.
- ^d Polarized basis of Ref. 33.
-

Once we have reliable estimates of the force at selected points it is important to employ an analytic representation which is capable of reproducing these forces. We developed a procedure, described in detail elsewhere [33], that involves only linear parameters and that fits exactly the input ab initio points at a set of r and χ values for each R, but that does not involve a truncated Legendre expansion of the potential. The avoidance of a truncated Legendre expansion of the potential, which has often been employed, is considered important because a Legendre expansion of the anisotropy may converge slowly in the repulsive region. The new functional form is based on a multiplicative correction to a pairwise additive potential. Truncating the Legendre expansion of the multiplicative correction is much less serious than truncating a Legendre expansion of the potential itself. It should be noted that for some values of R and χ , our analytic representation predicts the force to have the opposite sign than that predicted by the pairwise additive potential that serves as the original factor. Figure 5 shows the values of V_{int} and $-F_{\text{int}}$ on the two surfaces for the same collinear orientation as used for Figure 4.

3.2 HF + HF: a challenge for the dynamicist

In this subsection we discuss selected aspects of the quantum mechanical treatment of vibrational-to-vibrational (V-V) energy transfer in the collision of two hydrogen fluoride (HF) molecules. V-V energy transfer has long been a topic of widespread interest for dynamicists because of the possibility of resonant or near-resonant transitions, which have large probabilities and dominate nonequilibrium energy relaxation under many circumstances. An

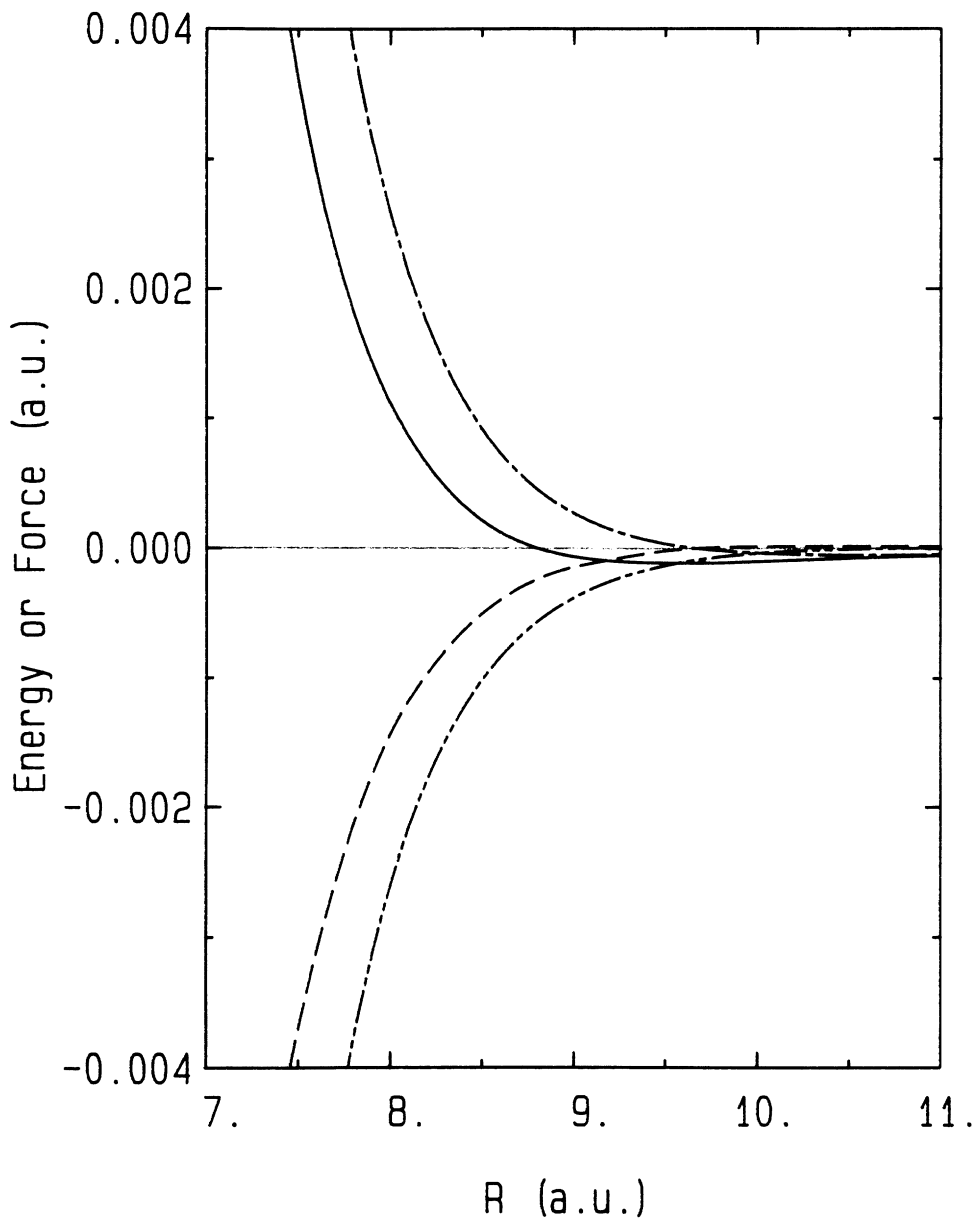


Figure 5. V_{int} and F_{int} for $\text{He} + \text{I}_2$ with $r = r_e$ and $\chi = 0^\circ$: solid curve, V_{int} of Ref. 33; long-short dashed curve, V_{int} from Ref. 36; dashed curve, $-F_{\text{int}}$ from Ref. 33; long-short-short dashed curve, $-F_{\text{int}}$ of Ref. 36.

important question in interpreting the large transition probabilities often observed for V-V energy transfer is ascertaining the respective roles and relative importance of short-range versus long-range forces. Early calculations on V-V energy transfer were performed using simple interaction potential functions, such as a nearest-neighbor exponential repulsions or truncated multipole series, and were based on simplified treatments of the dynamics, such as perturbation theory. However, to draw reliable conclusions, it is necessary to use both accurate interaction potentials and accurate dynamics. The system that has received most attention is HF - HF, partly because of its technological importance and partly because of the availability of a convenient source of excitation. In the present discussion we restrict ourselves to this one most studied system.

Several HF - HF potentials have been proposed on the basis of ab initio calculations [135-141]. Until recently, the most accurate of these were based on the Hartree-Fock, double-zeta-plus-polarization calculations of Yarkony et al. [142] of the interaction potential for two HF molecules, both at the diatomic equilibrium internuclear separation, but at various distances and relative orientations with respect to each other. In order to extend these calculations to predict the dependence on vibrational coordinates, Poulsen, Billing, and Steinfeld [136] fit them to a sum of two-center terms (the reliability of this kind of extension is suspect). More recently Binkley and Redmon [38] have produced a new potential energy surface. This is an improvement over all previous analytic representations in that it is based on a set of ab initio points that include varying HF distances and also in that it was computed using a larger one-electron basis set (6-311G**) and including electron correlation at the level of fourth-order Møller-Plesset perturbation theory. The ab initio points were fit [38] to a functional form made up of the sum of two-body, three-body, and four-body terms (similar to that used previously for H₂O [143]), and it includes a large number of adjustable parameters. This

makes the potential expensive to evaluate, but it is probably unavoidable to use a complicated fit in order to accurately represent all of the important regions of the potential.

In performing classical trajectory calculations, the evaluation of the potential and its derivatives can become the most time-consuming part of the calculations, and one strives hard for a functional representation that is economical to evaluate. Dynamics calculations employing quantum mechanics do not involve nearly as large a percentage of the effort in the potential subroutine, though, so in the quantal case there is less emphasis on achieving an economical fit than on achieving a reliable one. In quantal dynamics calculations one expands the angular part of the interaction potential in terms of some complete set of functions which then allows the analytic evaluation of some integrals necessary for the calculation of matrix elements of the potential. The expansion we have used for our calculations is

$$V(\vec{R}, \vec{r}_1, \vec{r}_2) = \sum_{q_1 q_2 \mu} v_{q_1 q_2 \mu}(R, r_1, r_2) Y_{q_1 q_2 \mu}(\hat{r}_1, \hat{r}_2) \quad (7)$$

$$Y_{q_1 q_2 \mu}(\hat{r}_1, \hat{r}_2) = \frac{4\pi}{[2(1 + \delta_{\mu 0})]^{1/2}} [Y_{q_1 \mu}(\hat{r}_1) Y_{q_2 -\mu}(\hat{r}_2) + Y_{q_1 -\mu}(\hat{r}_1) Y_{q_2 \mu}(\hat{r}_2)] \quad (8)$$

where \vec{R} is the vector connecting the centers of masses of the two molecules, \vec{r}_i is the vector along the bond of molecule i in the coordinate system where the z axis is in the direction of \vec{R} , and $Y_{q\mu}$ is a spherical harmonic. This form was chosen because it is completely general and yet it depends only on the six independent quantities $R, r_1, r_2, \theta_1, \theta_2$, and $\phi_1 - \phi_2$, where θ_i and ϕ_i are the inclination and azimuthal angles of r_i with respect to the vector \vec{R} . The coefficients $v_{q_1 q_2 \mu}$ are determined numerically for each value of R, r_1 , and r_2 required for a calculation, and a large

number of them are necessary to accurately reproduce $V(\bar{R}, \bar{r}_1, \bar{r}_2)$. In our scattering calculations we retain a maximum of 161 terms in Eqn. (7). We keep all terms with $q_1 + q_2 \leq 10$ [note that $\mu \leq \min(q_1, q_2)$] and use 11-point quadrature in each of the three angles θ_1 , θ_2 , and $\phi_1 - \phi_2$ to determine the 161 coefficients. This requires the evaluation of $V(\bar{R}, \bar{r}_1, \bar{r}_2)$ at a total of 1331 different angles for each value of R , r_1 , and r_2 required, which is far greater than the number of angles used in generating the analytic representation $V(\bar{R}, \bar{r}_1, \bar{r}_2)$. Since our quantum mechanical scattering calculations require the potential at about 1.5×10^4 sets of R , r_1 and r_2 , it would require about two million words of memory or mass storage to hold the required potential information in the form of Eqn. (7). Thus we recompute it from the original multi-center fit for each scattering calculation. One important aspect of using an expansion like this is that the work of evaluating the potential function is independent of the number of coupled channels included in the quantal scattering calculation, although only when a large number of coupled channels (>100) are considered does the potential function evaluation take less than half of the total time for a scattering calculation at one energy.

Although there are superficial similarities between the Poulsen-Billing-Steinfeld (PBS) [136] surface and the Binkley-Redmon (BR) [38] one, they can give quite different energy transfer probabilities. To illustrate this we have performed some calculations using a model [144] in which the two HF molecules are treated as breathing spheres. Table 6 gives the probabilities computed from these breathing-sphere calculations for the process $\text{HF}(v_1=1) + \text{HF}(v_2=1) \rightarrow \text{HF}(v_1=0 \text{ or } 2) + \text{HF}(v_2=2 \text{ or } 0)$. The effective spherical potential for the breathing sphere calculations was obtained first from the PBS surface and then from the BR surface, in each case using the potential corresponding to collinear intermolecular approach with the hydrogen end of molecule 2 approaching the fluorine end of molecule 1 (this is a hydrogen-bonding orientation).

Table 6. V-V energy transfer probabilities for HF-HF scattering in the breathing sphere model at a relative transitional energy of 0.03 eV.

Orbital angular momentum	Poulsen et al. P.E.S. ^a		Binkley-Redmon P.E.S. ^b	
	P _{11→02}	P _{11→20}	P _{11→02}	P _{11→20}
0	6.5(-2) ^c	3.7(-3)	2.8(-2)	7.2(-4)
12	6.5(-2)	3.6(-3)	2.7(-2)	6.4(-4)
24	6.4(-2)	3.3(-3)	2.5(-2)	4.2(-4)
36	6.4(-2)	2.8(-3)	2.1(-2)	1.3(-4)
48	6.2(-2)	2.2(-3)	1.6(-2)	3.6(-5)
60	5.8(-2)	1.5(-3)	1.0(-3)	1.0(-3)
72	5.1(-2)	8.0(-4)	4.3(-3)	5.1(-3)
84	4.0(-2)	2.3(-4)	7.9(-4)	1.2(-2)
96	1(-12)	1(-15)	1(-9)	4(-7)

^a using the potential energy surface of Ref. 136

^b using the potential energy surface of Ref. 38.

^c 6.5(-2) = 6.5 x 10⁻².

The calculations show that the V-V energy transfer probabilities for the breathing sphere calculations in which the potential is based on the PBS surface slowly decrease as the relative orbital angular momentum quantum number increases from zero up to about $\ell = 96$, where they suddenly drop several orders of magnitude. This sudden drop occurs when the centrifugal barrier becomes large enough to prevent (classically) the molecules from getting close enough together to feel the hard core repulsion of the potential. The probabilities from the BR surface are quite different for ℓ in the range 0 to 96: the P_{11→20} probability decreases as ℓ increases from 0 to 48, but then increases dramatically as ℓ further increases from 60 to 84.

In the previous section it was pointed out that it is possible to correlate the square of the force along the oscillator coordinate at the classical turning point with vibrational excitation probability in He + I₂ collisions. The analog of this correlation for a V-V energy

transfer problem is to correlate the square of the product of the forces on each bond with the transition probability. Figure 6 shows a test of this correlation for the HF - HF system by plotting the logarithm of $P_{11 \rightarrow 20}$ or $P_{11 \rightarrow 02}$ as a function of the logarithm of the square of the product of the forces on each molecule, i.e., versus the logarithm of the quantity defined in Eqn. (6). The correlation is not as linear as was observed for HeI_2 , but the points in Figure 6 do for the most part lie in a small set of almost monotonic sequences, indicating that the forces do correlate strongly with the probabilities.

In an attempt to explain the quite different results predicted using potentials based on the the two surfaces, in Figure 7 we have plotted the forces as a function of the center-of-mass separation of the two molecules. Also shown is the interaction potential. For both surfaces the force on the first molecule is positive for large separations and slowly increases as the separation decreases until a maximum is reached at about $6 a_0$. At smaller distances the force decreases rapidly and goes to a very large negative number.

The situation is different for the second molecule. The PBS surface gives a force that is positive everywhere and increases as the separation decreases, while the RB surface gives a positive force for both large and small separations with local maxima at about 3.5 and $7.5 a_0$ and a local minimum around $5 a_0$. We tentatively attribute the qualitatively different opacity-function shapes for the two interaction potentials to this qualitative difference in the behavior of the forces.

It would be interesting to know what accurate ab initio calculations predict for the forces. This would require using a larger one-electron basis and directly calculating ab initio energies at geometries close to where the forces are required, the former to reduce possible basis-set superposition errors (as discussed below) and the latter to ensure that the forces need not be obtained from global fits with possibly large local errors. An alternative way to reduce the additional possible error in the forces due to the fit would be to employ a fitting procedure similar to that discussed

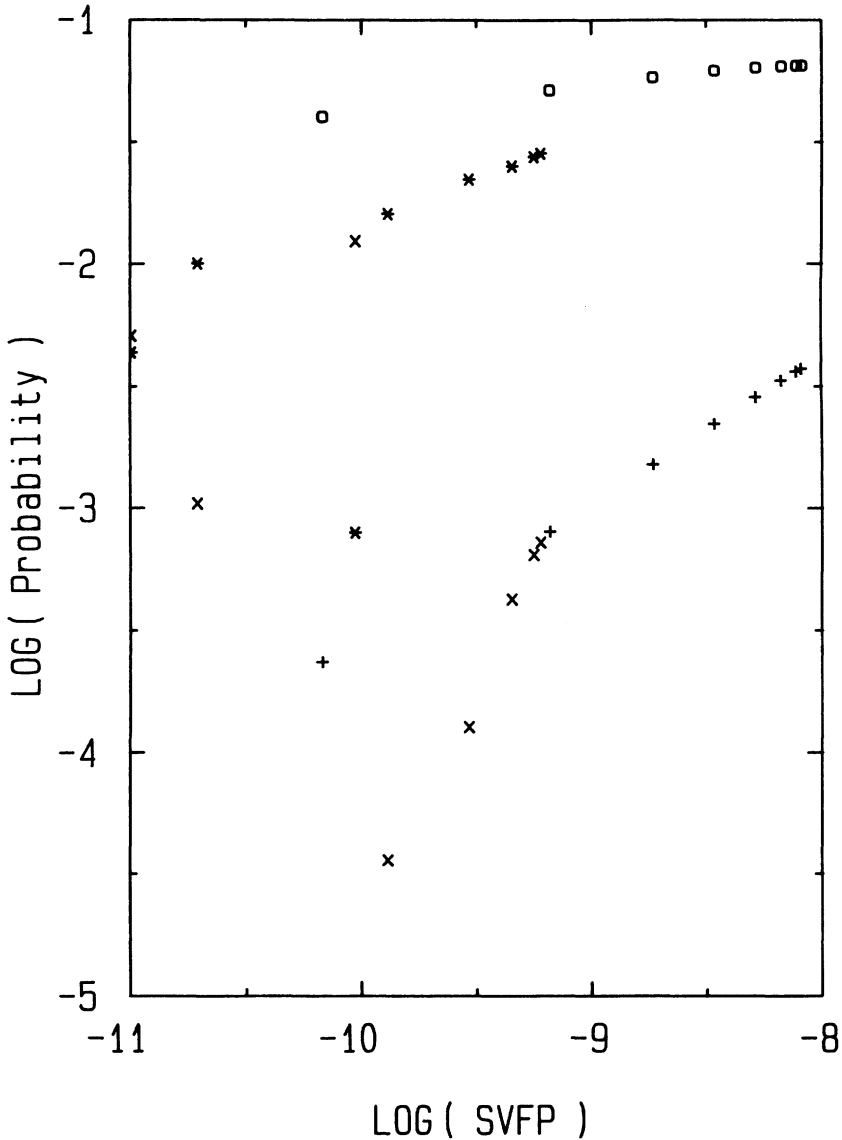


Figure 6. The logarithm of P_{11+20} and P_{11+02} for HF + HF as a function of the logarithm of the squared vibrational force product (SVFP) in a.u. for $E_{\text{rel}} = 0.030$ eV. This is from a breathing-sphere calculation with the potential from the collinear hydrogen-bonding orientation $H_1 - F_1 \dots H_2 - F_2$ (orientation I of Ref. 144); \square , P_{11+02} using PBS V_{int} ; $+$, P_{11+20} from PBS V_{int} ; \times , P_{11+02} from RB V_{int} ; $*$, P_{11+20} using RB V_{int} .

above for He - I₂; the kind of fit we used for He - I₂, as opposed to a more general multicenter fit, is designed to introduce minimal fitting error into the vibrational forces. It would also be interesting to replace the breathing-sphere calculations by converged quantal dynamics on the fully anisotropic (161-term) BR potential. Preliminary work on these full quantal dynamics calculations indicates that over 10³ coupled channels must be included for convergence, even with total angular momentum zero [34]. Further work on these large-scale dynamics calculations will be reported subsequently.

To learn more about the requirements on the one-electron basis set for accurate interaction potentials for the HF - HF system, we have done some restricted single-configuration Hartree-Fock calculations with a large number of basis sets for selected geometries of this system [37]. Our calculations used small, medium, large, and very large gaussian basis sets, and we attempted to assess the effect of basis-set superposition error on the calculation of interaction energies. Included in our calculations are the basis sets used by Yarkony et al. [142] and Binkley [38]. For the collinear hydrogen bonding approach, we considered a geometry with $R = 4 a_0$. The basis of Yarkony et al. [142] gave an energy of 16.2 kcal/mol, and the basis used by Binkley [38] gave an interaction energy of 16.6 kcal/mol, while our best estimate of the Hartree-Fock limit of the interaction energy is 18.5 ± 0.5 kcal/mol. Our large basis sets on which we base this estimate include more diffuse functions than either of the above basis sets, and these diffuse functions are important for reducing basis-set superposition error and for treating polarizability contributions to long-range interactions. Although we have not calculated the force predicted by these basis sets, it would be interesting to do so and include this information in the construction of an even more accurate potential energy surface for HF - HF collisions. We note that the BR fit at the hydrogen-bonding collinear geometry with $r_1 = r_2 = 1.723 a_0$ and $R = 4.0 a_0$ yields 13.07 kcal/mol, and the PBS fit at this geometry yields 4.73 kcal/mol. The ab initio calculations

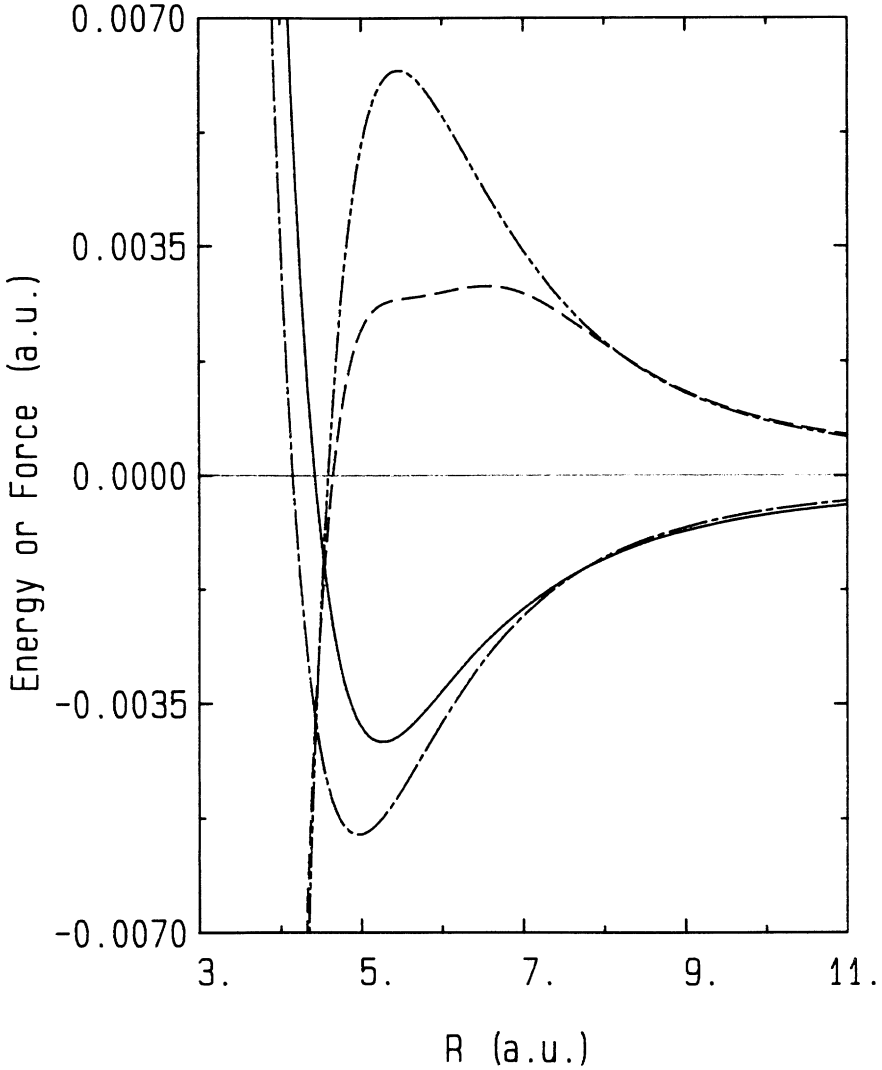


Figure 7a.

Figure 7. V_{int} and F_{int} for HF - HF collisions with $r_1 = r_2 = r_e$ in the same $H_1 - F_1 \dots H_2 - F_2$ orientation as used for Figure 6. In both part a and part b, the solid line is the RB V_{int} , and the long-short dashed line is the PBS V_{int} . a) dashed curve, $F_{\text{int}}^{(1)}$ from RB V_{int} ; long-short-short dashed curve, $F_{\text{int}}^{(1)}$ from PBS V_{int} . b) dashed curve, $F_{\text{int}}^{(2)}$ from RB V_{int} ; long-short-short dashed curve, $F_{\text{int}}^{(2)}$ from PBS V_{int} .

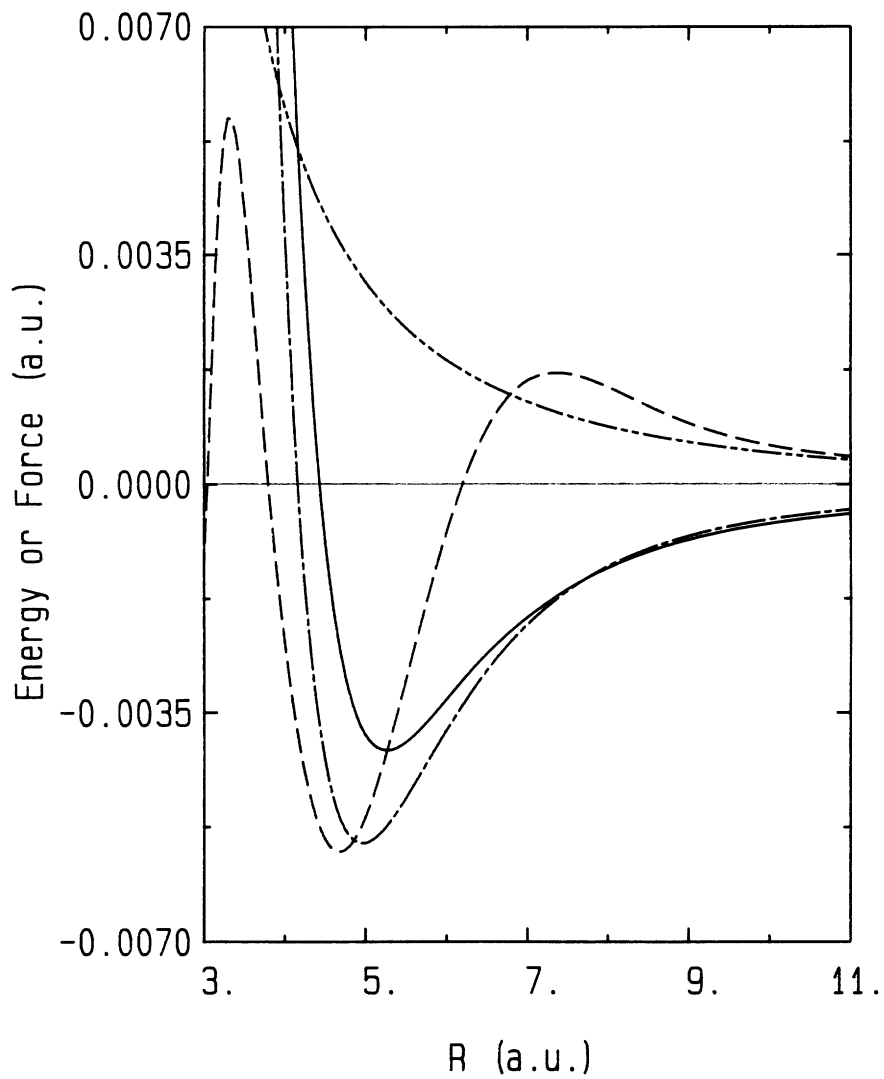


Figure 7b.

would appear to totally rule out the PBS value, but the difference between 18.5 and 13.1 kcal/mol may be a consequence of the inclusion of dispersion contributions in the BR surface.

4. CONCLUDING REMARKS

In this chapter we have reviewed some recent ab initio calculations of interaction potentials and whole potential energy surfaces and their use for studying molecular collisions. We have pointed out that in many cases some aspects of the dynamical results can be related to rather specific features of the potential energy surfaces. This is important because it allows one to concentrate on the convergence of these specific surface features rather than on convergence of the whole potential energy surface. One does still, however, require a global fit to the surface to perform full dynamics calculations, and we have also briefly discussed some new functional forms that may be useful for such fits. An important question discussed here, but still far from settled, is the reliability of various levels (methods + basis sets) of electronic structure calculations for various potential energy surface features.

5. ACKNOWLEDGMENTS

The authors are grateful to Professor Isaiah Shavitt for helpful discussions. The work at the University of Minnesota, except for variational transition state theory, is supported in part by the National Science Foundation under grant no. CHE8317944 and by a computing time grant from the Minnesota Supercomputer Institute. The work at the University of Minnesota on variational transition state theory is supported in part by the U.S. Department of Energy, Office of Basic Energy Sciences, under contract no. 79ER10425. The work at Chemical Dynamics Corporation is supported in part by the U.S. Army Research Office under contract no. DAAG-29-84-C-0011.

References:

1. B.C. Garrett and D.G. Truhlar, Proc. Natl. Acad. Sci. U.S.A., 76, 4755 (1979).
2. B.C. Garrett and D.G. Truhlar, J. Chem. Phys. 72, 3460 (1980).
3. B.C. Garrett, D.G. Truhlar, R.S. Grev. and A.W. Magnuson, J. Phys. Chem. 84, 1730 (1980).
4. N.C. Blais, D.G. Truhlar and B.C. Garrett, J. Phys. Chem. 85, 1094 (1981).
5. N.C. Blais and D.G. Truhlar: 1981, in "Potential Energy Surfaces and Dynamics Calculations," Ed. D.G. Truhlar, Plenum, New York, p. 431.
6. B.C. Garrett, D.G. Truhlar and R.S. Grev, *ibid*, p. 587.
7. B.C. Garrett and D.G. Truhlar, J. Phys. Chem. 86, 1136 (1982).
8. D.G. Truhlar, A.D. Isaacson, R.T. Skodje and B.C. Garrett, J. Phys. Chem. 86, 2252 (1982).
9. D.K. Bondi, D.C. Clary, J.N.L. Connor, B.C. Garrett and D.G. Truhlar, J. Chem. Phys. 76, 4986 (1982).
10. N.C. Blais, D.G. Truhlar and B.C. Garrett, J. Chem. Phys. 76, 2770 (1982).
11. N.C. Blais and D.G. Truhlar, Astrophys. J. 258, L79 (1982).
12. R.T. Skodje, D.G. Truhlar and B.C. Garrett, J. Chem. Phys. 77, 5955 (1982).
13. N.C. Blais and D.G. Truhlar, J. Chem. Phys. 78, 2388 (1983).
14. N.C. Blais, D.G. Truhlar and B.C. Garrett, 78, 2363 (1983).
15. D.G. Truhlar, R.S. Grev and B.C. Garrett, J. Phys. Chem. 87, 3415 (1983).
16. N.C. Blais and D.G. Truhlar, Chem. Phys. Lett. 102, 120 (1983).
17. B.C. Garrett and D.G. Truhlar, J. Chem. Phys. 81, 309 (1984).
18. B.C. Garrett and D.G. Truhlar, J. Phys. Chem., in press.
19. N.C. Blais, D.G. Truhlar and B.C. Garrett, J. Chem. Phys. 82, 2300 (1985).
20. A.D. Isaacson and D.G. Truhlar, J. Chem. Phys. 76, 1380 (1982).
21. D.G. Truhlar and A.D. Isaacson, J. Chem. Phys. 77, 3516 (1982).
22. A.D. Isaacson, M.T. Sund, S.N. Rai and D.G. Truhlar, J. Chem. Phys. 82, 1338 (1985).
23. B.C. Garrett, D.G. Truhlar, A.F. Wagner, and T.H. Dunning, Jr., J. Chem. Phys. 78, 4400 (1983).
24. S.N. Rai and D.G. Truhlar, J. Chem. Phys. 79, 6046 (1983).
25. D.G. Truhlar, K. Runge, and B.C. Garrett: In proceedings of Twentieth International Symposium on Combustion (August 12-17, 1984, Ann Arbor, Michigan), Combustion Institute, Pittsburgh, in press.
26. F.B. Brown, R. Steckler, D.W. Schwenke, D.G. Truhlar and B.C. Garrett, J. Chem. Phys. 82, 188 (1985).
27. R. Steckler, D.G. Truhlar and B.C. Garrett, J. Chem. Phys., in press.
28. R. Steckler, F.B. Brown and D.G. Truhlar, unpublished.
29. S. Green and D.G. Truhlar, Astrophys. J. 231, L101 (1979).

30. D.L. Thompson, N.C. Blais and D.G. Truhlar, *J. Chem. Phys.* 78, 1335 (1983).
31. D.G. Truhlar, *Bull. Amer. Phys. Soc.* 24, 70 (1979).
32. D.W. Schwenke and D.G. Truhlar, *J. Chem. Phys.* 81, 5586 (1984).
33. F.B. Brown, D.W. Schwenke and D.G. Truhlar, *Theoret. Chim. Acta*, in press.
34. D.W. Schwenke and D.G. Truhlar: in *Supercomputer Applications* (proceedings of the Supercomputer Applications Symposium, October 31–November 1, 1984, W. Lafayette, Indiana), Ed. R.W. Numrich, Plenum, New York, in press.
35. F.B. Brown and D.G. Truhlar, *Chem. Phys. Lett.* 113, 441 (1985).
36. D.W. Schwenke and D.G. Truhlar, *Chem. Phys. Lett.* 98, 217 (1983).
37. D.W. Schwenke and D.G. Truhlar, *J. Chem. Phys.* 82, 2418 (1985).
38. J.S. Binkley and M.J. Redmon, unpublished.
39. C.C.J. Roothaan, *Rev. Mod. Phys.* 32, 179 (1960).
40. I. Shavitt: 1977, in "Methods of Electronic Structure Theory," Vol. 1, Ed. H.F. Schaefer, III, Plenum, New York, p. 189.
41. B.O. Roos, P.R. Taylor and P.E.M. Siegbahn, *Chem. Phys.* 48, 157 (1980).
42. A. Veillard, *Theor. Chim. Acta* 4, 22 (1966).
43. G. Das and A.C. Wahl, *J. Chem. Phys.* 44, 3050 (1966).
44. J. Hinze and C.C.J. Roothaan, *Theor. Phys. Suppl.* 40, 37 (1967).
45. R.M. Pitzer, *J. Chem. Phys.* 58, 3111 (1973).
46. M. Dupuis, J. Rys and H.F. King, *J. Chem. Phys.* 65, 111 (1976).
47. R. Shepard, I. Shavitt and J. Simons, *J. Chem. Phys.* 76, 543 (1982).
48. H. Lischka, R. Shepard, F.B. Brown and I. Shavitt, *Int. J. Quantum Chem. Symp.* 15, 91 (1981).
49. W.L. Hase: 1981, in "Potential Energy Surfaces and Dynamics Calculations," Ed. D.G. Truhlar, Plenum, New York, p. 1; K. Morokuma and S. Kato, *ibid.*, p. 243; G.C. Schatz, *ibid.*, p. 287; T.H. Dunning, Jr., S.P. Walch and A.F. Wagner, *ibid.*, p. 329; D.A. Micha, *ibid.*, p. 685; J.C. Tully, *ibid.*, p. 805.
50. K. Fukui: 1983, in "New Horizons of Quantum Chemistry," Eds. P.-O. Lowdin and B. Pullman, Reidel, Dordrecht, p. 111; K. Morokuma, S. Kato, K. Kitaura, S. Obara, K. Ohta and M. Hanamura, *ibid.*, p. 221; M. Simonetta, *ibid.*, p. 295.
51. D.G. Truhlar, *Int. J. Quantum Chem. Symp.* 17, 77 (1983).
52. T.H. Dunning and L.B. Harding, in "The Theory of Chemical Reaction Dynamics," Ed. M. Baer, CRC Press, Boca Raton, FL, in press.
53. R.J. Heidner and J.F. Bott, *J. Chem. Phys.* 63, 1810 (1975).
54. J.F. Bott, *J. Chem. Phys.* 65, 1976 (1976).
55. F.E. Bartoszek, D.M. Manos and J.C. Polanyi, *J. Chem. Phys.* 69, 933 (1978).
56. C.F. Bender, B.J. Garrison and H.F. Schaefer, III, *J. Chem. Phys.* 62, 1188 (1975).
57. P. Botschwina and W. Meyer, *Chem. Phys.* 20, 43 (1977).
58. W.R. Wadt and N.W. Winter, *J. Chem. Phys.* 67, 3068 (1977).

59. A.F. Voter and W.A. Goddard, *J. Chem. Phys.* 75, 3638 (1981).
60. T.H. Dunning, *J. Phys. Chem.* 88, 2469 (1984).
61. P.J. Kuntz, E.M. Nemeth, J.C. Polanyi, S.D. Rosner and C.E. Young, *J. Chem. Phys.* 44, 1168 (1966).
62. J.T. Muckerman, *Theor. Chem. Adv. Perspectives* 6A, 1 (1981).
63. B.C. Garrett, D.G. Truhlar, R.S. Grev, G.C. Schatz and R.B. Walker, *J. Phys. Chem.* 85, 3806 (1981).
64. D.M. Neumark, A.M. Wodtke, G.N. Robinson, C.C. Hayden and Y.T. Lee: 1984, in "Resonances in Electron-Molecule Scattering, van der Waals Complexes, and Reactive Chemical Dynamics," Ed. D.G. Truhlar, American Chemical Society, Washington, p. 479.
65. D.M. Neumark, 1984, Ph.D. Thesis, University of California, Berkeley, unpublished.
66. Y.T. Lee, lecture presented at Fifth American Conference on Theoretical Chemistry, Grand Teton National Park, Wyoming, June 19, 1984.
67. A. Bunge, *J. Chem. Phys.* 53, 20 (1970).
68. S.R. Langhoff and E.R. Davidson, *Int. J. Quantum Chem.* 8, 61 (1974).
69. B. Liu, *J. Chem. Phys.* 80, 581 (1984).
70. (a) B. Liu, *J. Chem. Phys.* 58, 1925 (1973). (b) P. Siegbahn and B. Liu, *J. Chem. Phys.* 68, 2457 (1978). (c) D.G. Truhlar and C.J. Horowitz, *J. Chem. Phys.* 68, 2466 (1978); 71, 1514(E) (1979).
71. A.E. DeVries and F.S. Klein, *J. Chem. Phys.* 41, 3428 (1964).
72. G.O. Wood, *J. Chem. Phys.* 56, 1723 (1972).
73. J.D. McDonald and D.R. Herschbach, *J. Chem. Phys.* 62, 4740 (1975).
74. H. Endo and G.P. Glass, *Chem. Phys. Lett.* 44, 180 (1976).
75. F.S. Klein and I. Veltman, *J. Chem. Soc. Faraday Trans. II* 74, 17 (1978).
76. R.E. Weston, *J. Phys. Chem.* 83, 61 (1979).
77. W. Bauer, L.Y. Rusin and J.P. Toennies, *J. Chem. Phys.* 68, 4490 (1978).
78. W.H. Beck, R. Götzting, J.P. Toennies and K. Winkelmann, *J. Chem. Phys.* 72, 2896 (1980).
79. J.C. Miller and R.J. Gordon, *J. Chem. Phys.* 78, 3713 (1983).
80. C.A. Wight, F. Magnotta and S.R. Leone, *J. Chem. Phys.* 81, 3951 (1984).
81. D.L. Thompson, H.H. Suzukawa and L.M. Raff, *J. Chem. Phys.* 62, 4727 (1975).
82. T.H. Dunning, *J. Chem. Phys.* 66, 2752 (1977).
83. C.A. Parr and D.G. Truhlar, *J. Phys. Chem.* 75, 1844 (1971).
84. E.L. Mehler and W. Meyer, *Chem. Phys. Lett.* 38, 144 (1976).
85. J.H. Parker and G.C. Pimentel, *J. Chem. Phys.* 51, 91 (1969).
86. A. Ben-Shaul, Y. Haas, K.L. Kompa and R.D. Levine: 1981, in "Lasers and Chemical Change," Springer, Berlin.
87. R.D.H. Brown and A. Maitland, *Prog. React. Kinet.* 11, 1 (1981).
88. Y.T. Lee, *Ber. Bunsenges. Physik. Chem.* 86, 378 (1982).
89. R.E. Wyatt, J.F. McNutt and M.J. Redmon, *Ber. Bunsenges. Physik. Chem.* 86, 437 (1982).

90. K.L. Kompa and G.C. Pimentel, *J. Chem. Phys.* 47, 857 (1967); K.L. Kompa, J.H. Parker and G.C. Pimentel, *J. Chem. Phys.* 51, 91 (1969); R.D. Coombe and G.C. Pimentel, *J. Chem. Phys.* 59, 251 (1973).
91. J.C. Polanyi and D.C. Tardy, *J. Chem. Phys.* 51, 5717 (1969); K.G. Anlauf, P.E. Charters, D.S. Horne, R.G. MacDonald, D.H. Maylotte, J.C. Polanyi, W.J. Skrlac, D.C. Tardy and K.B. Woodall, *J. Chem. Phys.* 53, 4091 (1970); J.C. Polanyi and K.B. Woodall, *J. Chem. Phys.* 57, 1574 (1972).
92. T.P. Schaefer, P.E. Siska, J.M. Parson, F.P. Tully, Y.C. Wong and Y.T. Lee, *J. Chem. Phys.* 53, 3385 (1970).
93. N. Jonathan, C.M. Melliar-Smith and D.H. Slater, *Mol. Phys.* 20, 93 (1971); N. Jonathan, C.M. Melliar-Smith, D. Timlin and D.H. Slater, *Appl. Opt.* 10, 1821 (1971); N. Jonathan, C.M. Melliar-Smith, S. Okuda, D.H. Slater and D. Timlin, *Mol. Phys.* 22, 561 (1971).
94. W.H. Green and M.C. Lin, *J. Chem. Phys.* 54, 3222 (1971).
95. H.W. Chang and D.W. Setser, *J. Chem. Phys.* 58, 2298 (1973).
96. M.J. Berry, *J. Chem. Phys.* 59, 6229 (1973).
97. E. Wurzburg and P.L. Houston, *J. Chem. Phys.* 72, 4811 (1980).
98. R.F. Heidner, III, J.F. Bott, C.E. Gardner and J.E. Melzer, *J. Chem. Phys.* 72, 4815 (1980).
99. D.H. Neumark, A.M. Wodtke, G.N. Robinson, C.C. Hayden and Y.T. Lee, *Phys. Rev. Lett.* 53, 226 (1984).
100. C.F. Bender, P.K. Pearson, S.V. O'Neal and H.F. Schaefer, III, *J. Chem. Phys.* 56, 4626 (1972).
101. C.F. Bender, P.K. Pearson, S.V. O'Neal and H.F. Schaefer, III, *Science* 176, 1412 (1972).
102. S.R. Ungemach, H.F. Schaefer, III and B. Liu, *Discuss. Faraday Soc.* 62, 330 (1976).
103. P.D. Mercer and H.O. Pritchard, *J. Chem. Phys.* 63, 1468 (1959).
104. D.G. Truhlar and B.C. Garrett, *Acc. Chem. Res.* 13, 440 (1980).
105. B.C. Garrett and D.G. Truhlar, *J. Phys. Chem.* 83, 1079 (1979); 84, 682(E) (1980); 87, 4553(E) (1983).
106. B.C. Garrett, D.G. Truhlar, R.S. Grev, A.W. Magnuson and J.N.L. Connor, *J. Chem. Phys.* 73, 1721 (1980).
107. R.T. Skodje, D.G. Truhlar and B.C. Garrett, *J. Phys. Chem.* 85, 3019 (1982).
108. B.C. Garrett and D.G. Truhlar, *J. Chem. Phys.* 81, 309 (1984).
109. R. Steckler, D.G. Truhlar, B.C. Garrett, N.C. Blais and R.B. Walker, *J. Chem. Phys.* 81, 5700 (1984).
110. R.B. Walker and E.F. Hayes, *J. Phys. Chem.* 87, 1255 (1983).
111. D.G. Truhlar, B.C. Garrett and N.C. Blais, *J. Chem. Phys.* 80, 232 (1984).
112. D.L. Baulch, R.A. Cox, P.J. Crutzen, R.F. Hampson, Jr., J.A. Kerr, J. Troe and R.T. Watson, *J. Phys. Chem. Ref. Data* 11, 327 (1982).
113. R.J. Duchovic and W.L. Hase, *Chem. Phys. Lett.* 110, 474 (1984).
114. R.J. Duchovic, W.L. Hase, H.B. Schlegel, M.J. Frisch and K.

- Raghavachari, Chem. Phys. Lett. 89, 120 (1982).
115. R.J. Duchovic, W.L. Hase and H.B. Schlegel, J. Phys. Chem. 88, 1339 (1984).
116. G.B. Skinner, D. Rogers and K.B. Patel, Intern. J. Chem. Kinetics 13, 481 (1981).
117. F.B. Brown, I. Shavitt and R. Shepard, Chem. Phys. Lett. 105, 363 (1984).
118. Y.P. Varshni, Rev. Mod. Phys. 29, 664 (1957).
119. D. Steele, E.R. Lippincott and J.T. Vanderslice, Rev. Mod. Phys. 34, 239 (1962).
120. L. Halonen and M.S. Child, Mol. Phys. 46, 239 (1982).
121. L. Halonen and M.S. Child, J. Chem. Phys. 79, 4355 (1983).
122. S. Peyerimhoff, M. Lewerenz and M. Quack, Chem. Phys. Lett. 109, 563 (1984).
123. G.A. Baker and J.L. Gammell, The Padé Approximant in Theoretical Physics (Academic Press, New York, 1970).
124. W. Meyer, P.C. Hariharan and W. Kutzelnigg, J. Chem. Phys. 73, 1880 (1980).
125. M.H. Alexander and E.V. Berard, J. Chem. Phys. 60, 3950 (1974).
126. M.D. Gordon and D. Secrest, J. Chem. Phys. 52, 120 (1970).
127. J.W. Duff and D.G. Truhlar, J. Chem. Phys. 63, 4418 (1975).
128. G. Hall, K. Liu, M.J. McAuliffe, C.F. Giese and W.R. Gentry, J. Chem. Phys. 78, 5260 (1983); J. Chem. Phys. 81, 5577 (1984).
129. L.R. Kahn, P. Baybutt and D.G. Truhlar, J. Chem. Phys. 65, 3826 (1976).
130. T.P. Tsien and R.T. Pack, Chem. Phys. Lett. 6, 54 (1970).
131. M.A. Brandt and D.G. Truhlar, Chem. Phys. Lett. 23, 48 (1973).
132. W.R. Wadt and P.J. Hay, J. Chem. Phys. 82, 284 (1985).
133. R.E. Smalley, L. Warton and D.H. Levy, J. Chem. Phys. 68, 671 (1978).
134. See e.g. D.C. Clary, Chem. Phys. 65, 247 (1982); Mol. Phys. 51, 1299 (1984).
135. M.H. Alexander and A.E. DePristo, J. Chem. Phys. 65, 5009 (1976).
136. L.L. Poulsen, G.D. Billing and J.I. Steinfeld, J. Chem. Phys. 68, 5121 (1978).
137. W.L. Jorgensen and M.E. Cournoyer, J. Amer. Chem. Soc. 100, 4942 (1978).
138. W.L. Jorgensen, J. Chem. Phys. 70, 5888 (1980).
139. R.L. Redington, J. Chem. Phys. 75, 4417 (1981).
140. F.A. Gianturco, V.T. Lamanna and F. Battaglia, Int. J. Quantum Chem. 19, 217 (1981).
141. A.E. Barton and B.J. Howard, Discuss. Faraday Soc. 73, 45 (1982).
142. D.R. Yarkony, S.V. O'Neil, H.F. Schaefer, III, G.P. Baskin and C.F. Bender, J. Chem. Phys. 60, 855 (1974).
143. M.J. Redmon and G.C. Schatz, Chem. Phys. 54, 365 (1981).
144. D.W. Schwenke, D. Thirumalai, D.G. Truhlar and M.E. Coltrin, J. Chem. Phys. 78, 3078 (1983).